applied sciences

MDPI

Article

Finite Element Model Updating of Axisymmetric Structures

Pavol Lengvarský [1], Martin Hagara [1,*], Lenka Hagarová [2] and Jaroslav Briančin [2]

[1] Department of Applied Mechanics and Mechanical Engineering, Faculty of Mechanical Engineering, Technical University of Košice, Letná 1/9, 042 00 Košice, Slovakia; pavol.lengvarsky@tuke.sk
[2] Institute of Geotechnics of the Slovak Academy of Sciences, Watsonova 45, 040 01 Košice, Slovakia; hagarova@saske.sk (L.H.); briancin@saske.sk (J.B.)
* Correspondence: martin.hagara@tuke.sk

Abstract

Creating the most accurate numerical models with the same dynamic behavior as real structures plays an important role in the development process of various facilities. This article deals with the use of experimental methods, particularly experimental modal analysis (EMA), scanning, detection, spectral analysis, and mechanical testing in combination with the optimization techniques of the ANSYS 2024 R1 software to calibrate numerical models of axisymmetric structures. The proposed methodology was tested on a steel pipe whose geometric and material properties were both available. Within the updating of finite element models (FEMU) with one or two design variables, the influence of the range of feasible values on the accuracy of the observed parameters was examined. The updating process led to the acquisition of such a pipe model, which natural frequencies differed by less than 1.5% from the results estimated in EMA, and its weight also differed only minimally. The proposed methodology was then used for the FEMU of a pressure vessel whose contour was obtained by a 3D scanning method; material properties were investigated, and all wall thicknesses, i.e., eleven design variables, were unknown and thus determined by an iterative optimization technique. Using the Multi-Objective Genetic Algorithm (MOGA) method, the dimensions of the vessel were first updated for their shell model and subsequently for the 3D model. The resulting natural frequencies of the model with applied internal pressures of 0 bar, 40 bar, and 80 bar differed from those estimated experimentally by less than 1.2%.

Keywords: experimental modal analysis; modal parameters; finite element analysis; finite element model updating; optimization; axisymmetric structure; pipe; vessel

check for updates

Academic Editor: Tiago Filipe da Silva Miranda

Received: 25 September 2025
Revised: 20 October 2025
Accepted: 22 October 2025
Published: 24 October 2025

Citation: Lengvarský, P.; Hagara, M.; Hagarová, L.; Briančin, J. Finite Element Model Updating of Axisymmetric Structures. *Appl. Sci.* **2025**, *15*, 11407. https://doi.org/10.3390/app152111407

Copyright: © 2025 by the authors. Licensee MDPI, Basel, Switzerland. This article is an open access article distributed under the terms and conditions of the Creative Commons Attribution (CC BY) license (https://creativecommons.org/licenses/by/4.0/).

1. Introduction

The finite element method (FEM) is an integral part of numerical analyses of various structures used for stress control, optimization, prediction, damage identification, and others. However, despite its wide application, significant differences often arise between numerical results and experimental measurements, caused by idealizations of geometry, material properties, or boundary conditions. In the case of analyses of the dynamic behavior of structures, differences may arise between the natural frequencies, reaching up to several tens of percent [1,2], which significantly limits the usability of such models for reliable dynamic analysis. For this reason, a method known as finite element model updating (FEMU) has been developed to match the results obtained by numerical modeling with experimental ones. In general, the FEMU process can be formulated as an optimization task where the difference between the numerical and experimental dynamic responses of

the structure is minimized. Such characteristics include natural frequencies and modal shapes, which provide detailed information on both the global and local behavior of the structure in terms of weight and stiffness distribution.

FEMU methods can be divided into two categories, i.e., one-step (also referred to as direct methods) and iterative methods. One-step methods directly modify (in a one-step procedure) the elements of the mass and stiffness matrix of the analytical model, thereby accurately reproducing experimental data. However, matrices updated in this way have little physical meaning and cannot be related to the physical properties of the finite element model [3]. On the other hand, iterative methods modify material or geometric characteristics through a step-by-step optimization process, which adjusts the physical properties of the FE model.

Significant pioneering works in the field of FEMU were carried out in the late 1970s and early 1980s. They are associated with authors such as Baruch and Bar-Itzhack [4] or Berman and Nagy [5,6], focusing on the development of direct techniques, considering the adjustment of system matrix elements based on a mathematical approach. While the first-named offered a principle based on updating the FE stiffness matrix and eigenvectors, the second laid the foundation for methods that update both mass and stiffness matrices of the system sequentially. The basic methodologies of direct and iterative methods using modal data and FRFs from the 1980s to the early 1990s were systematically summarized and developed by Friswell and Mottershead [3,7] and Lin and Ewins [8,9]. Contributions from this era formed the basis for the formulation of approaches based, for example, on frequency response function (FRF) data [10], substructure [11], or the inverse eigensensitivity method (IESM). In 2011, Mottershead et al. [12] provided some tutorial examples to realize FEMU based on the sensitivity method. The aforementioned approaches were further developed and used in tasks with more accurate modeling of the boundary conditions and damping influence, or in solving the nonlinear systems.

Currently, FEMU approaches still use results from experimental or operational modal analysis. Operational modal analysis, which is used less frequently, is mainly related to the creation of accurate numerical models of civil engineering structures such as buildings or bridges. Lorenzoni et al. [13] investigated modal parameters of four towers belonging to the ancient aqueduct system in Pompeii. They used the iterative procedure for updating the values of the masonry moduli of elasticity and stiffnesses of foundation springs, providing information on the soil–structure interaction. The introduction of spring elements at tower foundations provided a better calibration of the elastic characteristics of masonry. Specifically, the moduli of elasticity of structures were adjusted by 81–266%. In some modes of vibration, the differences between natural frequencies were reduced to 1–3%. Despite this significant correction, some modes still had differences in frequencies of up to 30% or lower MAC values (10–50%). The chimney, dating back to 1950, characterized by the presence of major cracks, was analyzed by Bru et al. [14]. The numerical models, calibrated according to the results of the ambient vibration test, confirmed that the cracks do not affect the bending modes, as the coefficient of variation between the natural frequencies obtained experimentally and numerically reached the values of 4–10%. On the other hand, the cracks decreased the chimney's torsional stiffness significantly and the damaged state of the building is related to the local bending-torsional mode. An ambient vibration test was also carried out to obtain the dynamic characteristics of the Sungai Raia UHPC bridge [15]. A sensitivity-based updating method was used to resolve the inaccuracies in its U-girder and concrete deck moduli of elasticity, densities, Poisson's ratios, and boundary conditions to ensure no more than a 5% difference between the updated model and the actual model's natural frequencies. Moreover, the MAC values were equal to at least 90%. FEMU of the masonry minaret was performed with respect to the natural frequencies

and modal shapes obtained from OMA by Calayır et al. [16]. In this case, the moduli of elasticity of the minaret and soil were selected as design variables for model updating of the structure–foundation–soil system. The fact that the updating model was successful was evident from the reduction in frequency differences from the range of 12.6–22.8% to 2.9–3.4%. The analysis of a 53-story, 230 m tall structure in Qatar was presented by Avci et al. [17]. The authors realized several updates of the numerical model by decreasing its mass and increasing the modulus of elasticity. Simultaneously, partial releasing of the torsional restraint on columns and walls finally led to improved MAC values and decreased the differences between the compared natural frequencies. The resulting 22% decrease in mass and 25% increase in elastic modulus caused the average relative difference in natural frequencies to decrease from the initial 15.3% to 7.7%, or even 5.1% when excluding torsional modes. Zhao et al. developed an updated finite element model based on the results of the vibration tests performed on a steel frame structure subjected to road traffic loading [18]. Across most vibration modes, a good match between the updated finite element model and experimental measurements was obtained, with shape consistency greater than 80% and acceptable differences below 20%. In 2012, Ribeiro et al. [19] realized a calibration of a bowstring-arch railway bridge numerical model based on the results of an ambient vibration test. They used the natural frequencies, mode shapes, and damping coefficients of twelve global and local modes of bridge vibration. The optimization process based on a genetic algorithm was used to update the numerical model with 15 variables, whereby its robustness was demonstrated by achieving less than 5% frequency differences; MAC values were above 0.85, or even 0.9 for local modes. Vibration test data under base excitation were used to update the finite element models of the damped beam and satellite structures provided by Yuan and Yu [20]. Their innovative approach firstly updated the stiffness and mass parameters, and consequently, the damping. The authors also observed that parameters having a large difference in magnitude faced the updating problem. The proposal of the model for the prediction of the dynamic behavior of bolted joints in hybrid aluminum/composite structures was performed by Adel et al. [21]. They used the concept of the so-called joint affected region to prepare their doubly connective layer model to identify the modulus of elasticity in an isotropic metallic substructure, as well as the modulus in three directions in an anisotropic composite substructure. The updated model not only correlated precisely with the results obtained experimentally (average relative difference less than 0.9% observed in six modes) but also correctly predicted higher modes not included in the optimization process. Investigation of a composite panel made of unidirectional flax fibers embedded in a polyethylene matrix was carried out by Petrone and Meruane [22] using both mechanical testing and experimental modal analysis. They conducted modal tests using two approaches, i.e., modal hammer excitation with the response captured by miniature accelerometers and an electrodynamic shaker in cooperation with a vibrometer, whereby a more significant negative influence was observed by the use of the shaker. Their FE model was updated in two stages, i.e., globally and individually in 60 regions created, using an inverse modeling method based on parallel genetic algorithms, whereby more accurate results were obtained in the second stage. The FEMU of carbon/epoxy composite plates was performed by Cuadrado et al. [23]. The authors performed a sensitivity analysis based on the Montecarlo approach to increase the efficiency of the methodology by reducing the number of optimized variables. Their experimental modal analysis was very accurate, leading to the assessment of 22 natural frequencies and corresponding mode shapes. After FEMU, total error in frequencies dropped to only 0.6%. Experimental modal analysis of two different scenarios of the radioactive waste package prototype, i.e., an empty one and one hosting a dummy primary waste package, was carried out by Eiras et al. [24] to obtain data for updating the numerical

model, describing the dynamic mechanical behavior of the concrete containers. The genetic algorithm method was used to successfully calibrate the model, allowing even detection, localization, and quantification of damage severity in the containers based on modal analysis. Damage identification using the data from modal analysis and FE model updating was also carried out on reinforced concrete slabs by Dimri and Chakraborty [25], whereby an inverse eigensensitivity algorithm was implemented to minimize the weighted difference in the analyzed natural frequencies and modal shapes.

This article demonstrates the possibility of realizing such a calibration process, allowing for the determination of unknown geometric characteristics of the analyzed axisymmetric structures and updating of their FE models. In the case of axially symmetric structures, almost all modes are repeated, i.e., one is associated with the cosine mode of an integer wavenumber and the other with the sine mode of the same wavenumber. Any deviation from axial symmetry, mass, and stiffness leads to a split in the natural frequencies of the repeated modes, which may lead to negative consequences. For example, sensors exhibiting a slight deviation from axial symmetry may operate with reduced accuracy; in vehicle components, frequency split increases the possibility of resonance, contributing to a higher number of dangerous operating zones. The novelty of this article lies in the implementation of multiple input multiple output (MIMO) experimental modal analysis and the inclusion of repeated modes in the FEMU procedure, which is critical for axially symmetric bodies but is often neglected. The results of the experimental tests led to the acquisition of information about frequency splitting. Unlike most previously published works, the authors chose the multi-objective genetic algorithm method to minimize the difference between the selected natural frequencies, quantitatively comparing the frequencies of both repeated modes. Genetic algorithms (GAs) are currently often associated with industrial optimization problems that cannot be solved using traditional methods. These are mainly problems with a large or not well-understood search space [26]. In addition, GA-based methods are used, for example, in the optimization of manufacturing processes [27] and the design of metamaterial structures [28]. In this article, the reference analyses were performed on a steel pipe made of material with known mechanical properties, whose dimensions were easily identifiable by conventional measuring means. The validation of the methodology was implemented on a pressure vessel with a closed profile, which did not allow the thickness of its walls to be known. To improve the accuracy of the vessel numerical model, the authors designed and applied a comprehensive experimental–numerical process, including scanning, detection, spectral analysis, and mechanical testing, combined with numerical methods with potential for industrial use.

2. Materials and Methods

The reference analysis was carried out on a cylindrical-shaped structure, which was prepared for measurement by cutting off the end of the D_w 120 flue pipe at a distance of 100 mm from its narrowed part (Figure 1). The length of the analyzed structure was thus L_m = 900 mm. The pipe was made of DC01 steel, which was surface-treated with heat-resistant black spray paint with a nominal wall thickness of T = 1.5 mm. The weight of the analyzed structure was determined using a Hyundai KVE893B scale (Eta a.s., Prague, Czech Republic) with a capacity of 5000 g and a division of 1 g, with a resulting value of 3916 g obtained from three repeated measurements.

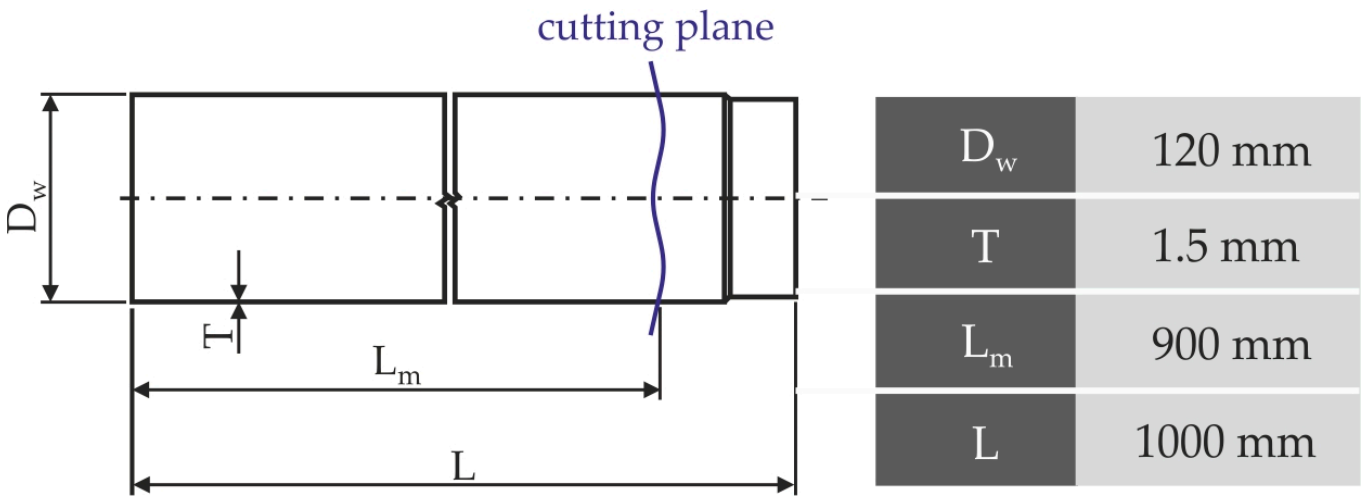


Figure 1. The analyzed pipe and its dimensions before and after preparation (cutting off the narrowed part) for measurement.

Experimental modal data of the pipe captured in the form of frequency response functions (FRFs) were obtained using the Brüel & Kjær Pulse® system with an LAN-XI module type 3050 (Hottinger Brüel & Kjær A/S, Virum, Denmark) specialized in vibration analysis. The control and execution of measurements were performed in the Pulse MTC Hammer V.21.0.0 software (Hottinger Brüel & Kjær A/S, Virum, Denmark), in which a simplified geometry of the analyzed pipe was created (Figure 2).

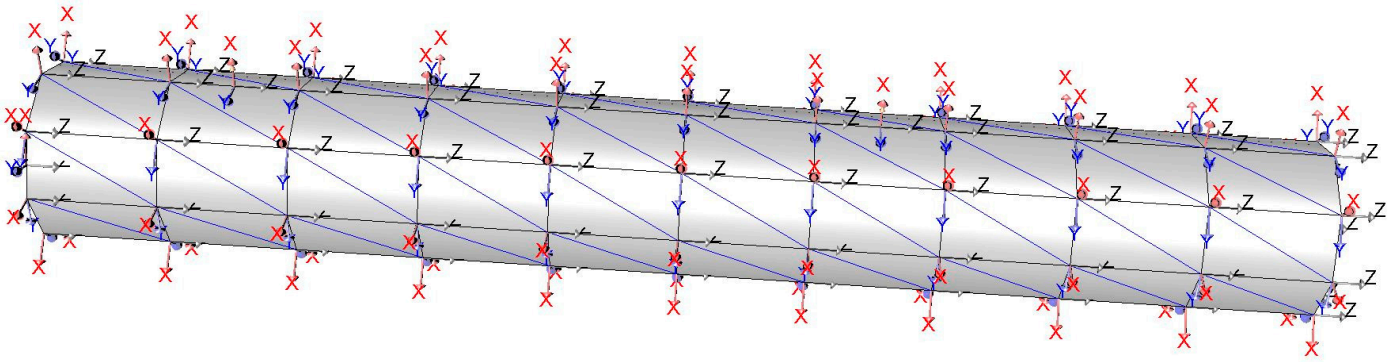


Figure 2. Geometry of the analyzed pipe created in the Pulse MTC Hammer software.

In order to compare the modal parameters obtained experimentally with those obtained numerically, it was necessary to establish measurement conditions that would allow for a free-free test and eliminate the impact of fixture modes, friction, and most damping, respectively. Such constraints are typically considered to be, for example, soft springs, foam pads, but also flexible rubber strings, which were used to hang the pipe on a rigid frame (Figure 3).

Measurements using the fixed embedded accelerometer and roving hammer-impact method were performed by the Brüel & Kjær 8206 impact hammer (Hottinger Brüel and Kjær A/S, Virum, Denmark) with a plastic tip, which was used to gradually excite 88 measuring points (degrees of freedom, DOFs) evenly distributed across the outer surface of the pipe. This impact hammer, having an output voltage sensitivity of 22.7 mV/N and full-scale force range compression of 220 N, is suitable for impact force measurements implemented on small to medium structures. The response of the structure was registered in directions X and Y, respectively, at three reference DOFs (Figure 3) using Brüel and Kjær 4507B piezoelectric uniaxial accelerometers (Hottinger Brüel and Kjær A/S, Virum,

Denmark). Each of the DOFs was excited three times, and the resulting signals were obtained using the linear peak hold average method of the fast Fourier transform (FFT) signals, leading to an increase in the accuracy of the obtained FRFs.

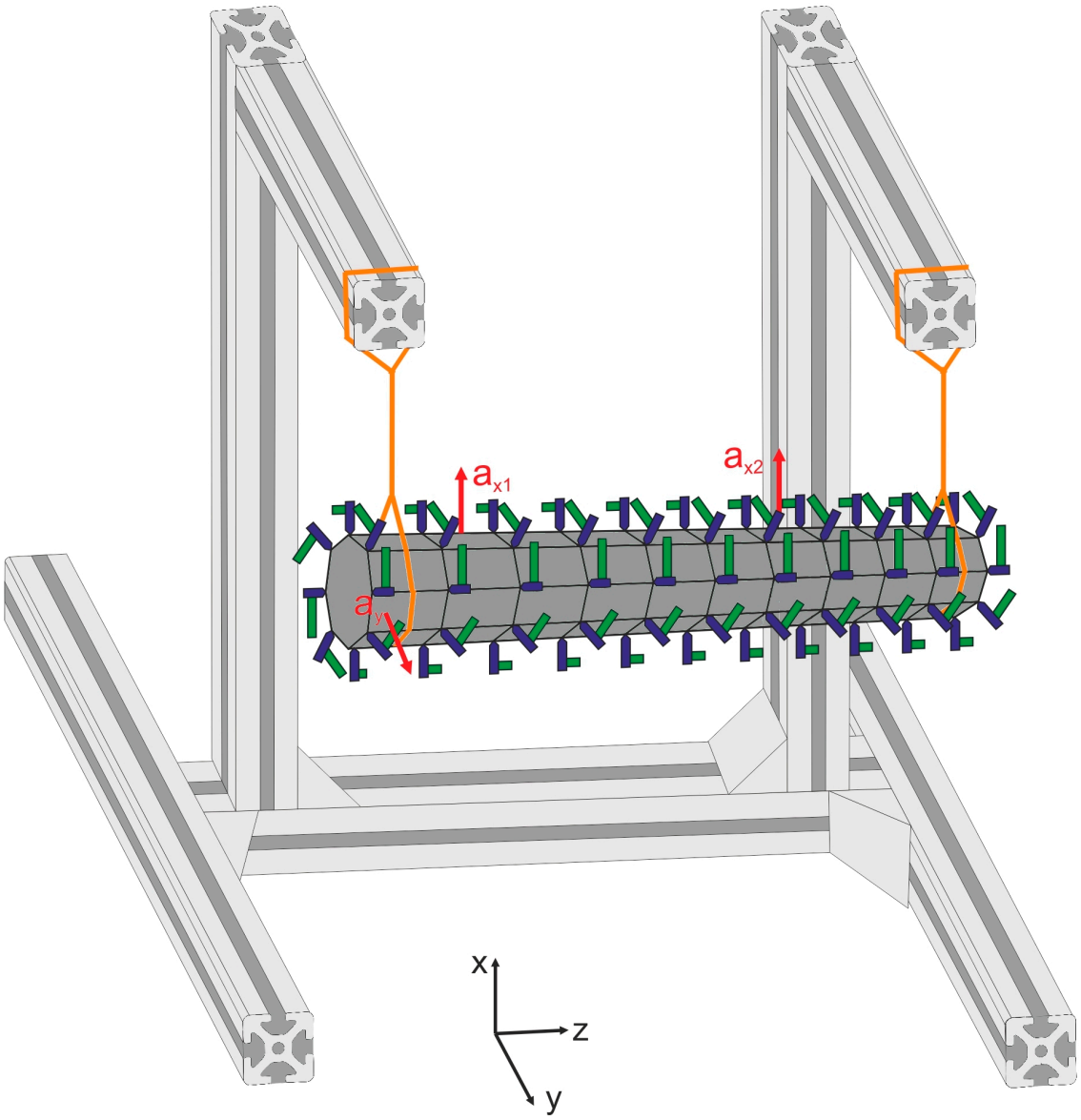


Figure 3. Schematic representation of DOFs (locations of hammers), reference DOFs (red arrows), and free-free constraint of the analyzed pipe provided by the flexible rubber strings (orange).

The evaluation of the 88 obtained FRFs was performed in the Pulse Reflex® V.21.0.0 software (Hottinger Brüel & Kjær A/S, Virum, Denmark), whereby the values of natural frequencies, damping ratios, and modal shapes of the vessel's individual modes in the frequency span of 0–1200 Hz were estimated with a frequency resolution of 1.25 Hz.

2.1. Estimation of the Pipe Modal Parameters

Since three uniaxial accelerometers were used to capture the response of the analyzed pipe, it was expected that information about its closely spaced or repeated modes, typical for axisymmetric structures, would also be obtained. Since the frequencies of these modes differ only minimally, instead of a set of FRFs, methods belonging to the Mode Indicator Function (MIF) group, e.g., Complex Mode Indicator Function (CMIF), are required to be

used to estimate and separate them. The estimation process of modes will be explained using a CMIF plot obtained from the pipe modal analysis (Figure 4).

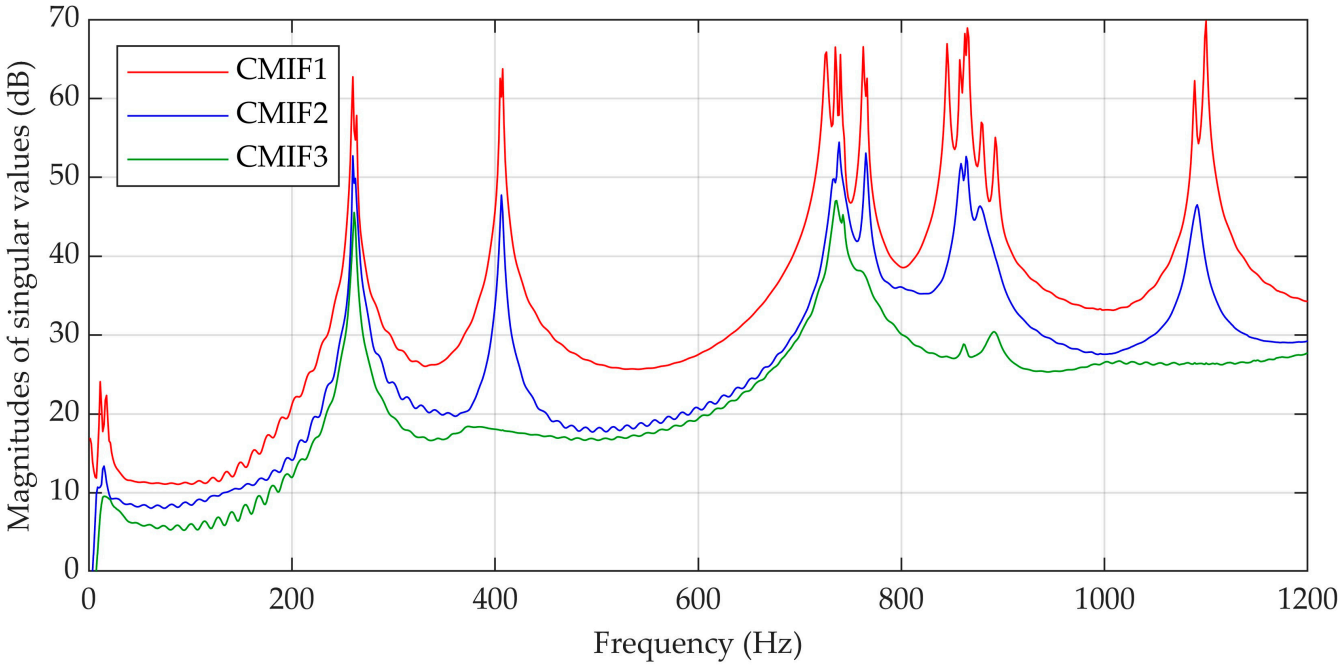


Figure 4. Three singular curves of the CMIF plot obtained from experimental modal analysis of the pipe in the frequency span of 0–1200 Hz.

The first peaks in the CMIF plot were obtained in the frequency span around 11–17 Hz. For that reason, a stability diagram was plotted using the Rational Fraction Polynomial-Z method for the selected frequency span of 0–40 Hz to identify the poles of stability. Based on the modal shapes observed, it was determined that these modes represent so-called rigid modes of the pipe's vibration. The first deformation modes were thus detected in the frequency span of 260–410 Hz. Based on the most stable poles in the selected frequency span of 200–500 Hz, modes with frequencies of 260 Hz, 263 Hz, 405 Hz, and 407 Hz were determined as possible modes of the pipe's vibration. Such a procedure was repeated several times and was used to identify all stable modes of the pipe in the frequency span of 0–1200 Hz. The identified modes of vibration were then checked using auto MAC (Figure 5).

This function allows correlations between modes to be established, with an emphasis on confirming that the selected modes with closely spaced natural frequencies correspond to so-called repeated modes. If the MAC value, calculated between two modal shape vectors $\boldsymbol{\Phi}_i$ and $\boldsymbol{\Phi}_j$ according to

$$\mathrm{MAC}(\boldsymbol{\Phi}_i, \boldsymbol{\Phi}_j) = \frac{\left|\boldsymbol{\Phi}_i^T \boldsymbol{\Phi}_j\right|}{\left(\boldsymbol{\Phi}_i^T \boldsymbol{\Phi}_j\right)\left(\boldsymbol{\Phi}_i^T \boldsymbol{\Phi}_j\right)} \tag{1}$$

is equal to 1, it represents identical modal shapes. On the other hand, an MAC value equal to 0 corresponds to completely distinct modal shapes. As seen in Figure 5, the off-diagonal elements are equal to very small values near zero, which confirms that the selected modes have close frequencies but distinct modal shapes. For this reason, it can be spoken about repeated modes. The estimated natural frequencies and damping ratios of the individual vibration modes of the pipe are shown in Tables 1 and 2. The experimental results show slight frequency splits. This effect is often related with unevenly distributed mass, stiffness, material anisotropy, or defects that disrupt the axial symmetry of the actual structure.

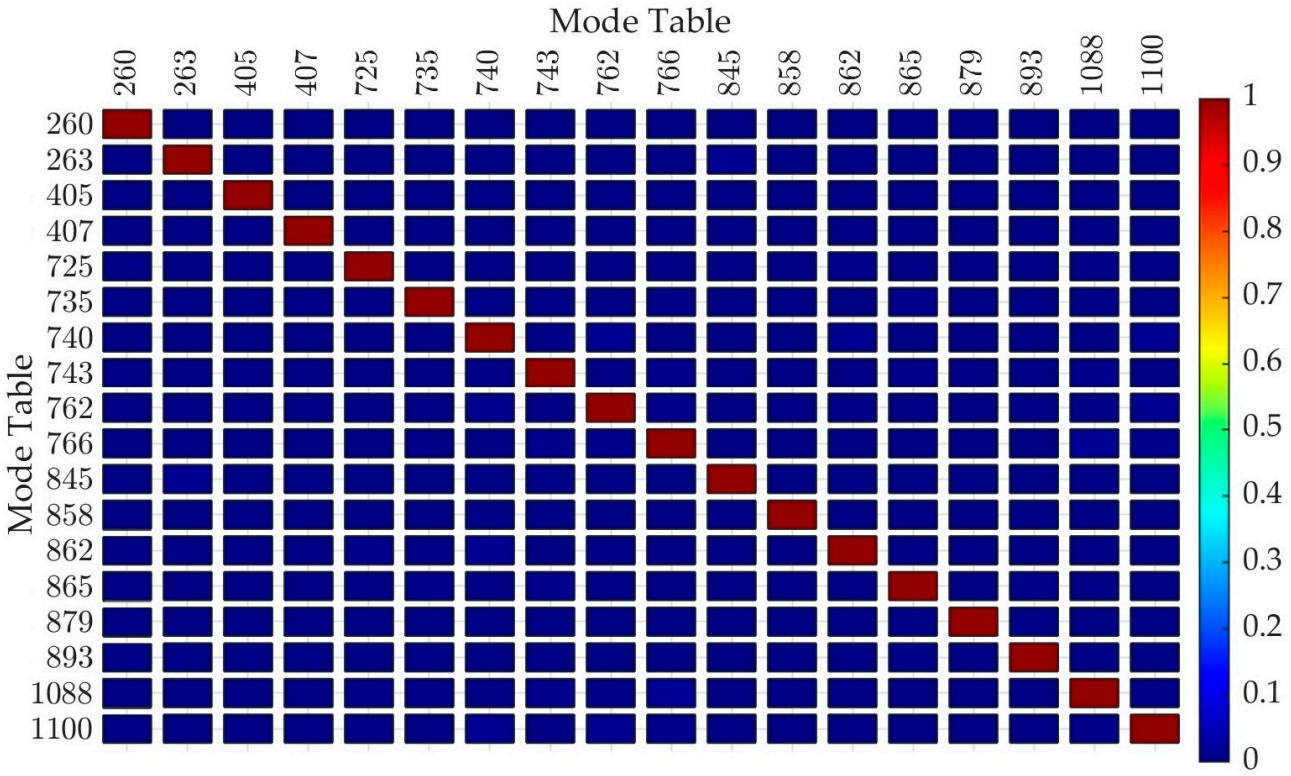


Figure 5. Auto MAC matrix of estimated modes of the pipe's vibration. An MAC value of 1 represents identical modal shapes; an MAC value of 0 corresponds to completely distinct modal shapes.

Table 1. Natural frequencies of the analyzed pipe estimated by EMA. $^{\alpha}$, $^{\beta}$ = repeated modes; † = mode was not found.

Estimated Natural Frequency (Hz)									
Mode 1	**Mode 2**	**Mode 3**	**Mode 4**	**Mode 5**	**Mode 6**	**Mode 7**	**Mode 8**	**Mode 9**	**Mode 10**
260	263	405 $^{\alpha}$	725 $^{\alpha}$	740 $^{\alpha}$	762 $^{\alpha}$	845 $^{\alpha}$	862 $^{\alpha}$	879 $^{\alpha}$	1088 $^{\alpha}$
†	†	407 $^{\beta}$	735 $^{\beta}$	743 $^{\beta}$	766 $^{\beta}$	858 $^{\beta}$	865 $^{\beta}$	893 $^{\beta}$	1100 $^{\beta}$

Table 2. Damping ratios of the analyzed pipe estimated by EMA. $^{\alpha}$, $^{\beta}$ = repeated modes; † = mode was not found.

Estimated Damping Ratio (%)									
Mode 1	**Mode 2**	**Mode 3**	**Mode 4**	**Mode 5**	**Mode 6**	**Mode 7**	**Mode 8**	**Mode 9**	**Mode 10**
0.1853	0.1951	0.1311 $^{\alpha}$	0.2349 $^{\alpha}$	0.0876 $^{\alpha}$	0.1173 $^{\alpha}$	0.1211 $^{\alpha}$	0.1051 $^{\alpha}$	0.1802 $^{\alpha}$	0.0930 $^{\alpha}$
†	†	0.1291 $^{\beta}$	0.0986 $^{\beta}$	0.0877 $^{\beta}$	0.0925 $^{\beta}$	0.0787 $^{\beta}$	0.0803 $^{\beta}$	0.1702 $^{\beta}$	0.0780 $^{\beta}$

The modal shapes of the pipe, observed for natural frequencies in the list in the first row of Table 1, estimated by EMA, are shown in Figure 6. It can be assumed that a higher number of DOFs selected on the pipe surface would improve their accuracy. Nevertheless, the modal shapes obtained in the selected frequency span of 0–1200 Hz are easily distinguishable and identifiable. An increased number of DOFs would also make the measurements more time-consuming, and probably no significant change in the estimated natural frequencies of the structure would be achieved [29]. It can also be stated that the number of modes obtained is sufficient for the correlation of the results obtained by the experimental and numerical modal analysis.

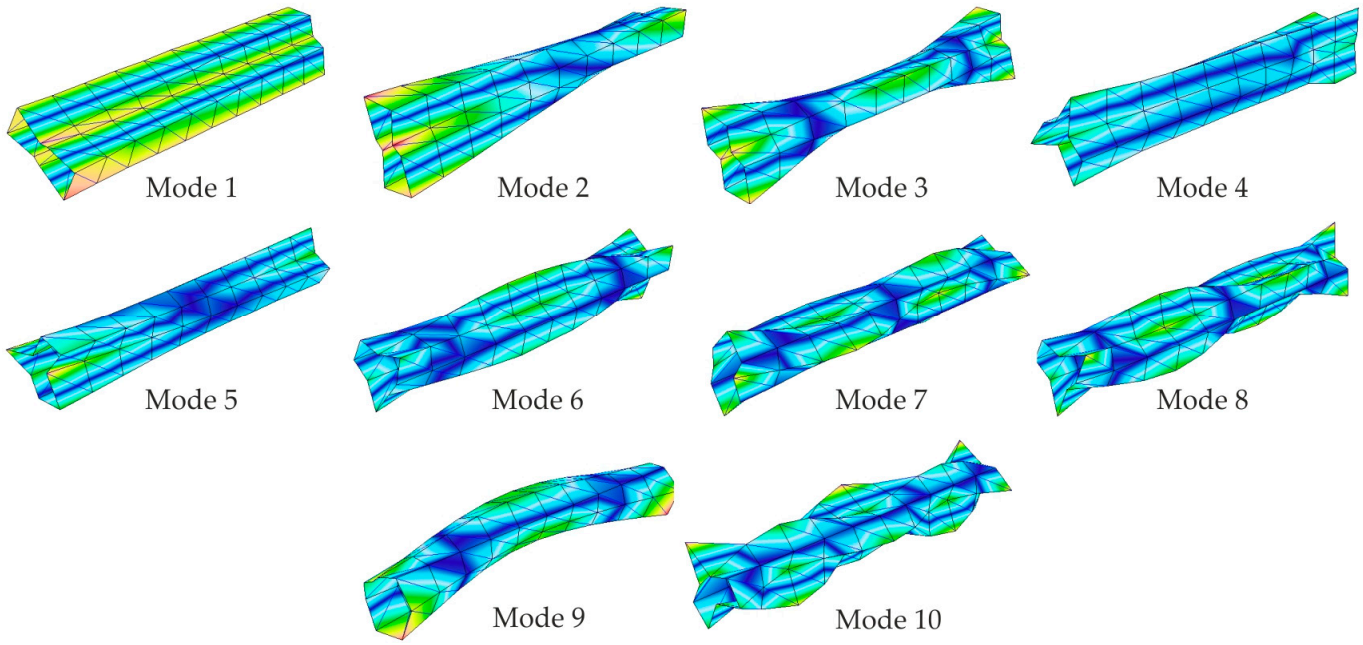


Figure 6. Modal shapes of the analyzed pipe estimated by EMA in the selected frequency span of 0–1200 Hz. For all the estimated repeated modes, the figure shows only one mode determined at the first singular curve of the CMIF plot.

2.2. Numerical Model of the Pipe and Its Updating

The numerical modal analysis based on the finite element method was performed in the ANSYS Mechanical 2024 R1 (Canonsburg, PA, USA) software. A free-free-constrained 3D model of a steel pipe with dimensions R_i = 60 mm (inner radius), R_o = 61.5 mm (outer radius), and L_m = 900 mm (length) was created. Material properties were assigned to the model, i.e., Young's modulus of elasticity E = 200,000 MPa, Poisson's ratio ν = 0.3, and density ρ = 7850 kg/m^3. The mesh independence analysis was carried out by analyzing the relative change in natural frequencies due to the varying size of the elements, number of divisions in radial direction, and full or reduced integration. For the selected elements defined sequentially with the sizes of 3 mm, 2 mm, 1 mm, and 0.5 mm, only minimal differences (much less than 0.1%) observed in natural frequencies were achieved, i.e., each of the analyzed mesh could be used. Finally, the authors decided to create a mesh containing two elements defined on the thickness of the pipe, consisting of 967,572 twenty-node hexahedral 3D solid elements (SOLID186) with quadratic approximation and reduced integration. The average size of elements created was 0.85 mm. With such defined parameters of the model, a numerical modal analysis was performed, the results of which served as initial information on modal parameters (natural frequencies and modal shapes) of the pipe's numerical model in the frequency span of 0–1200 Hz. The obtained initial values of the natural frequencies are given in Table 3.

Table 3. Natural frequencies of the initial pipe 3D model obtained by numerical modal analysis realized in ANSYS. $^{\alpha}$, $^{\beta}$ = repeated modes.

FEA–Natural Frequency (Hz)									
Mode 1	**Mode 2**	**Mode 3**	**Mode 4**	**Mode 5**	**Mode 6**	**Mode 7**	**Mode 8**	**Mode 9**	**Mode 10**
264.9 $^{\alpha}$	266.7 $^{\alpha}$	403.1 $^{\alpha}$	748.6 $^{\alpha}$	750.8 $^{\alpha}$	774.0 $^{\alpha}$	830.9 $^{\alpha}$	859.0 $^{\alpha}$	867.5 $^{\alpha}$	1084.1 $^{\alpha}$
264.9 $^{\beta}$	266.7 $^{\beta}$	403.1 $^{\beta}$	748.6 $^{\beta}$	750.8 $^{\beta}$	774.0 $^{\beta}$	830.9 $^{\beta}$	859.0 $^{\beta}$	867.5 $^{\beta}$	1084.1 $^{\beta}$

The mean difference Δ_{mean} between the natural frequencies obtained numerically and experimentally calculated according to

$$\Delta_{mean} = \frac{\sum_{i=1}^{n} \left| \left(\frac{f_{i\mathrm{FEM}}}{f_{i\mathrm{EMA}}} - 1 \right) \right|}{n} \cdot 100\%, \quad (2)$$

where n is the number of compared data, $f_{i\mathrm{FEM}}$ is the value of the i-th natural frequency obtained numerically, and $f_{i\mathrm{EMA}}$ is the value of the i-th natural frequency obtained experimentally, achieved a value of approximately 1.49%. The weight of the initial numerical model of the pipe was 4045 g, which represented a relative increase of approximately 3.3% in the weight of the model compared to the actual weight of the pipe (3916 g).

2.2.1. FEMU of the Pipe with One Design Variable

The pipe's FEMU, i.e., the changes in its geometry, was based on the modal parameters estimated by EMA and optimization techniques of the ANSYS Mechanical 2024 R1 software. In the first phase, only one design variable was considered, i.e., the outer radius of the pipe R_o, while the remaining two dimensions were defined as follows: inner radius R_i = 60 mm and pipe length L_m = 900 mm. For the analysis of the updated model accuracy, five ranges (Range 1 to Range 5) were selected step-wise and defined as feasible values of the design variable R_o (left part of Table 4). For selecting the most appropriate modes as optimization functions, the following criteria were defined:

- The selected modes are well identified within EMA, i.e., with stable poles, consistent modal shape, and reproducibility.
- The selected modes are separated and do not correspond to modes with closely spaced natural frequencies, so that they cannot be mistaken for each other.
- The selected modes have the highest participation factor from the FEA-obtained set of modes.

Table 4. Defined ranges of feasible values for the design variable R_o with the results of the optimization process in the form of three candidate points obtained by the ANSYS software.

	Design Variable R_o		**Optimization Results**		
Name	**Lower Bound**	**Upper Bound**	**Candidate Point 1**	**Candidate Point 2**	**Candidate Point 3**
Range 1	60.001 mm	67 mm	61.313 mm	61.313 mm	61.313 mm
Range 2	60.001 mm	63 mm	61.313 mm	61.313 mm	61.313 mm
Range 3	60.001 mm	62 mm	61.434 mm	61.434 mm	61.434 mm
Range 4	60.001 mm	61.8 mm	61.477 mm	61.478 mm	61.478 mm
Range 5	60.001 mm	61.6 mm	61.489 mm	61.500 mm	61.500 mm

In this case, the deformation modes 1, 3, and 6 best met these conditions. When defining the optimization objectives, one of the repeated modes was always selected, specifically the one found on the first singular curve, i.e., the mode with the highest frequency response. The optimization objectives were defined with equal priority as follows:

- To seek a target of 260 Hz for the natural frequency of the pipe's first deformation mode.
- To seek a target of 405 Hz for the natural frequency of the pipe's third deformation mode.
- To seek a target of 762 Hz for the natural frequency of the pipe's sixth deformation mode.

In this case, the weight of the pipe model was only taken as an observed parameter without a defined optimization objective. The Multi-Objective Genetic Algorithm (MOGA) method based on controlled elitism concepts with 96 estimated design points (eight samples per iteration, with a maximum of 12 iterations) was chosen for the optimization, with the

aim of finding the global optimum. Based on the parameters selected, ANSYS determined three candidate points for each selected range of feasible values, which are listed on the right side of Table 4.

Based on the candidate point values, the R_o dimension was adjusted, and numerical modal analyses of the updated models were performed again. A comparison of the results obtained can be seen in Table 5, which, in addition to the absolute values of the relative differences (marked as Diff. (%)) between the values of the corresponding natural frequencies obtained numerically and experimentally, also shows the weights of the updated numerical models. Although this was a relatively simple optimization task with one design variable, it can be stated that for the largest range of feasible values (Range 1), the least accurate results were achieved with Δ_{mean} equal to 8.04%. In this case, the weight of the pipe numerical model was also significantly lower than that of the actual structure, with a difference of 380 g (9.7%). On the other hand, by gradually reducing the range of R_o feasible values to Range 4 and Range 5, it was possible to achieve Δ_{mean} of about 1.3%. The weight difference between the last two updated numerical models and the actual structure was 67 g and 98 g, respectively (1.7% and 2.5%, respectively).

Table 5. Comparison of pipe's natural frequencies obtained by EMA and FEA after model updating based on the candidate point values calculated for different ranges of feasible values of the design variable R_o. $^{\alpha}$, $^{\beta}$ = repeated modes; † = mode was not found; # = difference was not calculated.

Mode	EMA m = 3916 g	FEA R_o = 61.313 mm m = 3536 g		FEA R_o = 61.434 mm m = 3866 g		FEA R_o = 61.477 mm m = 3983 g		FEA R_o = 61.489 mm m = 4014 g	
	Freq. (Hz)	Freq. (Hz)	Diff. (%)	Freq. (Hz)	Diff. (%)	Freq. (Hz)	Diff. (%)	Freq. (Hz)	Diff. (%)
1	260	232.6 $^{\alpha}$	10.55	253.5 $^{\alpha}$	2.51	260.9 $^{\alpha}$	0.34	263.0 $^{\alpha}$	1.14
	†	232.6 $^{\beta}$	#	253.5 $^{\beta}$	#	260.9 $^{\beta}$	#	263.0 $^{\beta}$	#
2	263	234.2 $^{\alpha}$	10.95	255.2 $^{\alpha}$	2.95	262.7 $^{\alpha}$	0.12	264.8 $^{\alpha}$	0.67
	†	234.2 $^{\beta}$	#	255.2 $^{\beta}$	#	262.7 $^{\beta}$	#	264.8 $^{\beta}$	#
3	405 $^{\alpha}$	380.8 $^{\alpha}$	5.97	395.1 $^{\alpha}$	2.44	400.3 $^{\alpha}$	1.16	401.8 $^{\alpha}$	0.79
	407 $^{\beta}$	380.8 $^{\beta}$	6.43	395.1 $^{\beta}$	2.92	400.3 $^{\beta}$	1.64	401.8 $^{\beta}$	1.28
4	725 $^{\alpha}$	657.5 $^{\alpha}$	9.31	716.5 $^{\alpha}$	1.17	737.4 $^{\alpha}$	1.71	743.3 $^{\alpha}$	2.52
	735 $^{\beta}$	657.5 $^{\beta}$	10.55	716.5 $^{\beta}$	2.51	737.4 $^{\beta}$	0.33	743.3 $^{\beta}$	1.13
5	740 $^{\alpha}$	659.4 $^{\alpha}$	10.89	718.6 $^{\alpha}$	2.89	739.6 $^{\alpha}$	0.06	745.4 $^{\alpha}$	0.73
	743 $^{\beta}$	659.4 $^{\beta}$	11.25	718.6 $^{\beta}$	3.29	739.6 $^{\beta}$	0.46	745.4 $^{\beta}$	0.32
6	762 $^{\alpha}$	683.0 $^{\alpha}$	10.36	741.9 $^{\alpha}$	2.64	762.8 $^{\alpha}$	0.10	768.6 $^{\alpha}$	0.87
	766 $^{\beta}$	683.0 $^{\beta}$	10.83	741.9 $^{\beta}$	3.15	762.8 $^{\beta}$	0.42	768.6 $^{\beta}$	0.34
7	845 $^{\alpha}$	783.1 $^{\alpha}$	7.33	826.3 $^{\alpha}$	2.22	829.2 $^{\alpha}$	1.87	830.1 $^{\alpha}$	1.77
	858 $^{\beta}$	783.1 $^{\beta}$	8.73	826.3 $^{\beta}$	3.70	829.2 $^{\beta}$	3.35	830.1 $^{\beta}$	3.25
8	862 $^{\alpha}$	818.3 $^{\alpha}$	5.07	837.5 $^{\alpha}$	2.85	857.0 $^{\alpha}$	0.58	858.9 $^{\alpha}$	0.36
	865 $^{\beta}$	818.3 $^{\beta}$	5.40	837.5 $^{\beta}$	3.18	857.0 $^{\beta}$	0.93	858.9 $^{\beta}$	0.70
9	879 $^{\alpha}$	857.9 $^{\alpha}$	2.40	858.6 $^{\alpha}$	2.32	858.8 $^{\alpha}$	2.29	862.4 $^{\alpha}$	1.88
	893 $^{\beta}$	857.9 $^{\beta}$	3.93	858.6 $^{\beta}$	3.85	858.8 $^{\beta}$	3.83	862.4 $^{\beta}$	3.42
10	1088 $^{\alpha}$	1012.9 $^{\alpha}$	6.90	1058.6 $^{\alpha}$	2.70	1075.2 $^{\alpha}$	1.18	1079.8 $^{\alpha}$	0.75
	1100 $^{\beta}$	1012.9 $^{\beta}$	7.92	1058.6 $^{\beta}$	3.76	1075.2 $^{\beta}$	2.25	1079.8 $^{\beta}$	1.84
Δ_{mean}:			8.04		2.84		1.26		1.32

The modal shapes of individual modes (Figure 7) of the updated pipe's numerical model corresponded qualitatively to those obtained by the experimental modal analysis (Figure 6).

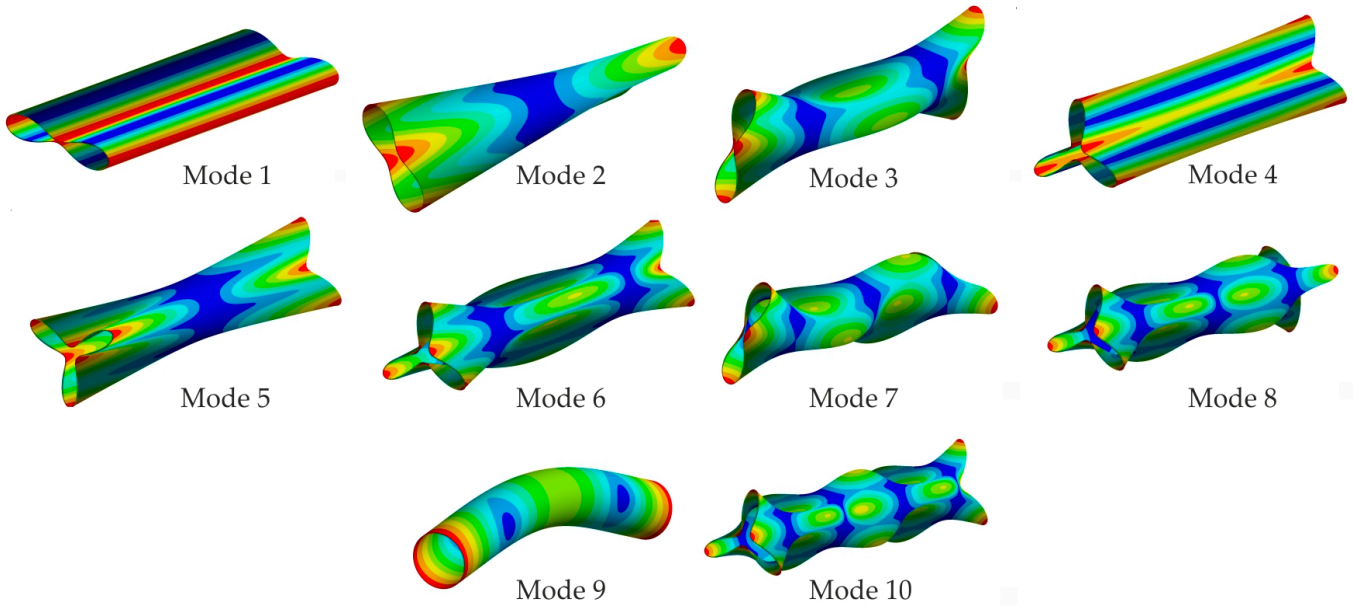


Figure 7. Deformation modal shapes of the updated pipe's numerical model obtained by FEA in the frequency span of 0–1200 Hz. For all the pairs of calculated repeated modes, the figure shows only the first, i.e., α mode.

2.2.2. FEMU of the Pipe with Two Design Variables

Since optimization tasks with one design variable are rare in technical practice, the authors decided to analyze the impact of various ranges of feasible values defined for more design variables on the accuracy. They considered that only the length of the pipe L_m = 900 mm was known, and both radii, i.e., the outer R_o and the inner R_i, were unknown. For the task with two design variables, three ranges of feasible values for R_i and R_o were defined according to the left part of Table 6. In this case, however, the optimization objectives were divided into the following:

A) The objectives with a higher priority are as follows:
- To seek a target of 260 Hz for the natural frequency of the first deformation mode;
- To seek a target of 3916 g for the mass of the pipe.

B) The objectives with a default priority are as follows:
- To seek a target of 405 Hz for the natural frequency of the third deformation mode;
- To seek a target of 762 Hz for the natural frequency of the sixth deformation mode.

Table 6. Defined ranges of feasible values for the design variables R_i and R_o, with the results of the optimization process in the form of three candidate points from the ANSYS software.

	Design Variable R_i		**Design Variable R_o**		**Optimization Results**		
Name	**Lower Bound**	**Upper Bound**	**Lower Bound**	**Upper Bound**	**Candidate Point 1**	**Candidate Point 2**	**Candidate Point 3**
Range 1	55.0 mm	60.0 mm	60.001 mm	65.0 mm	R_i = 59.799 mm R_o = 62.677 mm	R_i = 59.806 mm R_o = 62.694 mm	R_i = 59.824 mm R_o = 62.697 mm
Range 2	57.5 mm	60.0 mm	60.001 mm	62.5 mm	R_i = 59.620 mm R_o = 61.632 mm	R_i = 59.602 mm R_o = 61.583 mm	R_i = 59.589 mm R_o = 61.525 mm
Range 3	59.5 mm	60.5 mm	60.6 mm	62.0 mm	R_i = 59.500 mm R_o = 60.959 mm	R_i = 59.528 mm R_o = 60.986 mm	R_i = 59.535 mm R_o = 60.992 mm

The choice of selecting mass as one of the optimization functions was based on the results shown in Tables S1 and S2 (Supplementary Materials), where reducing the range

of feasible values of R_o and R_i to Range 3 did not further improve the results, and even led to their significant degradation. For this reason, it was considered to be appropriate to add another optimization function to the MOGA method, i.e., minimization of the difference between the numerical and actual mass of the pipe, which was chosen as a higher priority function together with minimizing the difference in deformation Mode 1 (dominant bending mode) frequency. With this strategy, convergence was achieved approximately 20% faster, and the results obtained were more in agreement with the results obtained in EMA.

The right part of Table 6 shows three candidate points determined by the ANSYS software for each defined range of feasible values. A comparison of the natural frequencies and masses of the updated models obtained numerically with experimentally obtained natural frequencies is shown in Table 7.

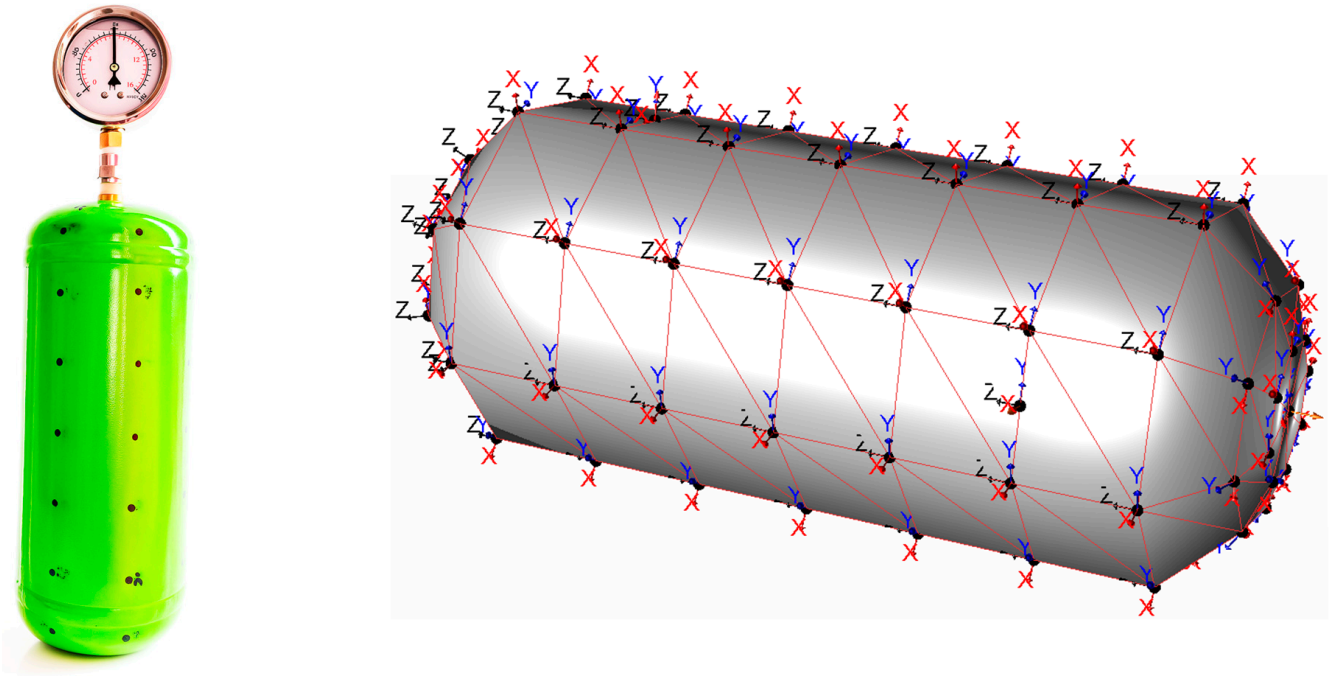
Table 7. Comparison of pipe's natural frequencies obtained by EMA and FEA after model updating based on the candidate point values calculated for different ranges of feasible values of the design variables R_i and R_o. $^{\alpha}$, $^{\beta}$ = repeated modes; † = mode was not found; # = difference was not calculated.

Mode	EMA m = 3916 g	FEA R_i = 59.824 mm R_o = 62.697 mm m = 7812 g		FEA R_i = 59.589 mm R_o = 61.525 mm m = 5204 g		FEA R_i = 59.528 mm R_o = 60.986 mm m = 3900 g	
	Freq. (Hz)	Freq. (Hz)	Diff. (%)	Freq. (Hz)	Diff. (%)	Freq. (Hz)	Diff. (%)
1	260	498.3 $^{\alpha}$	91.65	343.9 $^{\alpha}$	32.27	261.6 $^{\alpha}$	0.62
	†	498.3 $^{\beta}$	#	343.9 $^{\beta}$	#	261.7 $^{\beta}$	#
2	263	501.6 $^{\alpha}$	90.72	346.2 $^{\alpha}$	31.63	263.4 $^{\alpha}$	0.15
	†	501.6 $^{\beta}$	#	346.2 $^{\beta}$	#	263.4 $^{\beta}$	#
3	405 $^{\alpha}$	595.9 $^{\alpha}$	47.14	462.1 $^{\alpha}$	14.10	399.1 $^{\alpha}$	1.46
	407 $^{\beta}$	595.9 $^{\beta}$	46.41	462.1 $^{\beta}$	13.54	399.1 $^{\beta}$	1.94
4	725 $^{\alpha}$	865 $^{\alpha}$	19.31	856.8 $^{\alpha}$	18.18	739.5 $^{\alpha}$	2.00
	735 $^{\beta}$	865 $^{\beta}$	17.69	856.8 $^{\beta}$	16.57	739.5 $^{\beta}$	0.61
5	740 $^{\alpha}$	954.5 $^{\alpha}$	28.99	862.4 $^{\alpha}$	16.54	741.6 $^{\alpha}$	0.22
	743 $^{\beta}$	954.5 $^{\beta}$	28.47	862.4 $^{\beta}$	16.07	741.6 $^{\beta}$	0.19
6	762 $^{\alpha}$	1406.1 $^{\alpha}$	84.53	971.4 $^{\alpha}$	27.48	764.4 $^{\alpha}$	0.31
	766 $^{\beta}$	1406.2 $^{\beta}$	83.58	971.6 $^{\beta}$	26.84	764.5 $^{\beta}$	0.20
7	845 $^{\alpha}$	1410 $^{\alpha}$	66.86	974.1 $^{\alpha}$	15.28	824.3 $^{\alpha}$	2.45
	858 $^{\beta}$	1410 $^{\beta}$	64.34	974.3 $^{\beta}$	13.55	824.3 $^{\beta}$	3.93
8	862 $^{\alpha}$	1436.8 $^{\alpha}$	66.68	997.3 $^{\alpha}$	15.70	853.2 $^{\alpha}$	1.02
	865 $^{\beta}$	1436.8 $^{\beta}$	66.10	997.5 $^{\beta}$	15.32	853.2 $^{\beta}$	1.36
9	879 $^{\alpha}$	1513.4 $^{\alpha}$	72.17	1079.8 $^{\alpha}$	22.84	857.2 $^{\alpha}$	2.48
	893 $^{\beta}$	1513.4 $^{\beta}$	69.47	1079.9 $^{\beta}$	20.93	857.2 $^{\beta}$	4.01
10	1088 $^{\alpha}$	1559 $^{\alpha}$	43.29	1270.2 $^{\alpha}$	16.75	1072.7 $^{\alpha}$	1.41
	1100 $^{\beta}$	1559 $^{\beta}$	41.73	1270.3 $^{\beta}$	15.48	1072.7 $^{\beta}$	2.48
Δ_{mean}:			57.17		19.39		1.49

It can be stated that even in the case of two unknown design variables, it is possible to achieve a very good match between the natural frequencies of the actual structure and its numerical model (Δ_{mean} about 1.5%) and also in their weights (difference of only 16 g, or 0.4%). However, also in this case, it is necessary to select or gradually adjust (reduce) the specified range of design variables' feasible values to an adequate level and to add mass as an additional objective function if appropriate.

3. Validation of the Methodology

The validation of the described FEMU methodology was performed on the structure of a pressure vessel (Figure 8a). This differed from the pipe structure not only in its more complex shape, but also because its closed profile did not allow for knowing the thickness values of its individual parts, increasing the number of design variables. The known dimensions of the vessel were thus only its length of 260 mm (without valve) and outer radius of 51 mm. The weight of the vessel filled with gas, obtained by averaging the results of three weighs using a precision digital XS balance, model BL 2002 (Giorgio Bormac s.r.l., Carpi, Italy), with a capacity of 2000 g, division of 0.01 g, and repeatability of 0.01 g, was determined to be 1716 g.



(**a**) (**b**)

Figure 8. Analyzed pressure vessel: (**a**) actual structure with glycerin pressure gauge applied; (**b**) geometry of vessel model created in Pulse MTC Hammer V.21.0.0.

Determination of the modal parameters of the vessel at three loading states, i.e., filled with helium at the pressures of 80 bar, 40 bar, and 0 bar (or a very low internal pressure caused by the remaining unvented helium), was performed. The internal pressure was determined using a POLMO MGH63KG14D160P glycerin pressure gauge (POLMOstrów, Ostrów Wielkopolski, Poland) with a bottom connection, with a 0–160 bar range and ±1.6% accuracy class (Figure 8a), which had to be connected to the vessel via a thread-reducing nut. The frequency response of the vessel was captured using the same measuring equipment as described in Section 2. The measurements were performed using the Pulse MTC Hammer V.21.0.0 software (Hottinger Brüel & Kjær A/S, Virum, Denmark), in which the simplified geometry of the pressure vessel (Figure 8b) was created.

The vessel was freely suspended using soft rubber strings attached to a rigid frame by means of hooks (Figure 9). The fixed embedded accelerometer and roving hammer-impact method was again used to acquire the FRFs, with the excitation of 88 DOFs evenly distributed across the entire surface of the vessel, performed using a Brüel&Kjær 8206 impact hammer (Hottinger Brüel & Kjær A/S, Virum, Denmark) with a plastic tip.

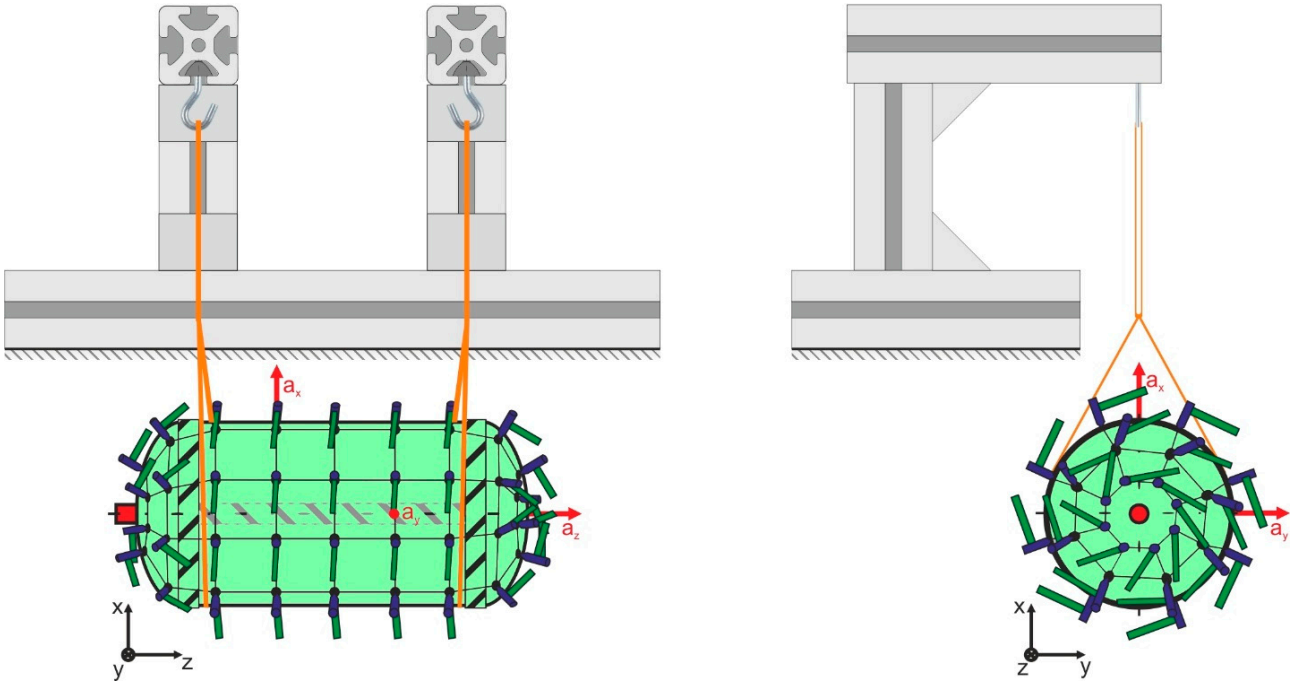


Figure 9. Schematic representation of DOFs (locations of hammers), reference DOFs (red arrows), and free-free fixture of the analyzed pressure vessel provided by the flexible rubber strings.

The response of the vessel was acquired sequentially in three reference DOFs. The Brüel & Kjær 4374 uniaxial miniature accelerometer (Hottinger Brüel & Kjær A/S, Virum, Denmark) was used to capture the response in mutually perpendicular directions X, Y, and Z. Each of the DOFs was excited three times, and the resulting signals were obtained by the linear peak hold average method of the FFT signals. The evaluation of 264 frequency response functions was performed in the Pulse Reflex® software, obtaining information on the natural frequencies, damping ratios, and modal shapes of the individual vessel vibration modes in the frequency span of 0–6400 Hz with a frequency resolution of 1 Hz.

3.1. Estimation of the Pressure Vessel Modal Parameters

The pressure vessel filled with helium was tested at three different levels of internal pressure, i.e., 80 bar, 40 bar, and 0 bar. Since a miniature accelerometer was used to register the response of the axially symmetric structure in mutually perpendicular directions X, Y, and Z, respectively, the assumption about repeated modes obtained was confirmed in all estimated vibration modes of the vessel, excluding one. The modes were estimated in the same way as described in Section 2.1, i.e., using CMIF. The CMIF plot of a vessel filled with helium at 80 bar pressure is shown in Figure 10.

The Rational Fraction Polynomial-Z method was used to identify the stability poles. Since some modes were not directly related to the vibration of the pressure vessel, but only to its valve, these modes were removed from the estimated ones. In the case of a vessel loaded with an internal pressure of 80 bar, these modes corresponded to the following frequencies: 2021 Hz, 3436 Hz, and 3440 Hz. The selected modes were checked in each measurement using the auto MAC. Figure 11 shows the auto MAC matrix of the modal shapes of the vessel loaded with an internal pressure of 80 bar. Based on the obtained MAC values, it is possible to conclude that there is a higher level of correlation between repeated modes (frequencies equal to 4533 Hz and 4536 Hz, or 6347 Hz and 6356 Hz), but also between more distant modes (2490 Hz and 6347 Hz, or 2489 Hz and 6356 Hz).

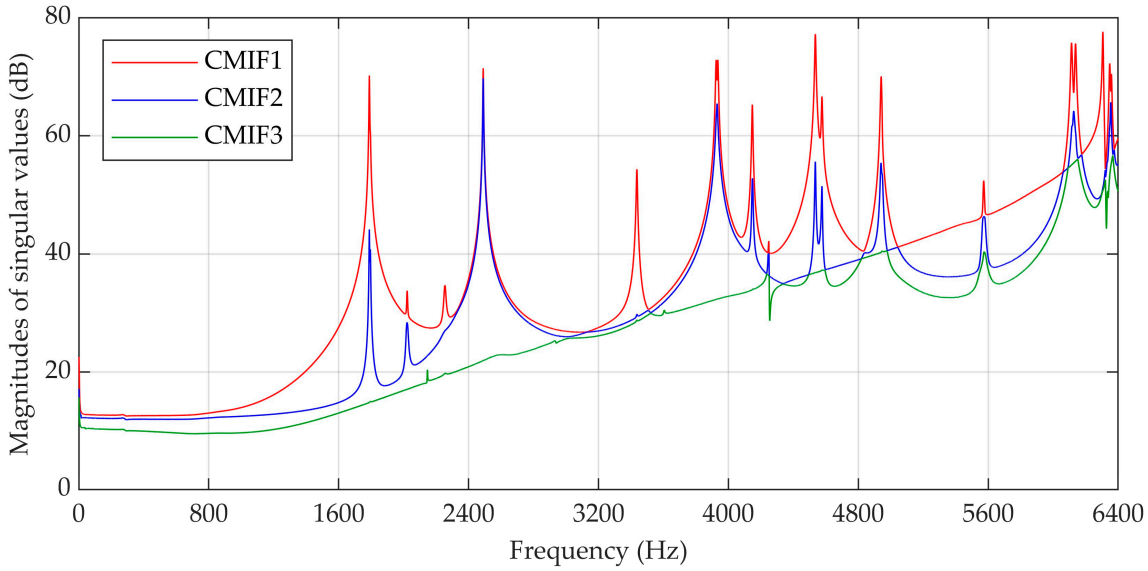


Figure 10. Three singular curves of the CMIF plot obtained from experimental modal analysis of the pressure vessel (80 bar).

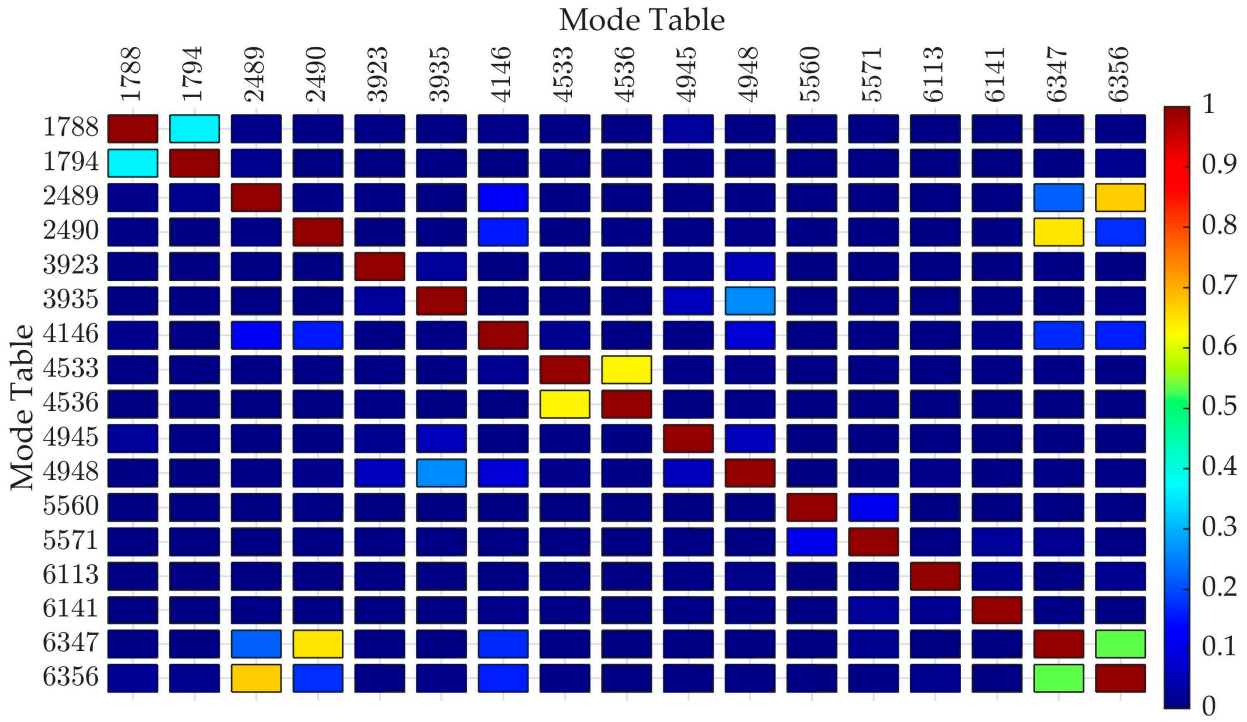


Figure 11. Auto MAC matrix of estimated modes of the pressure vessel filled with helium (80 bar). An MAC value of 1 represents identical modal shapes; an MAC value of 0 corresponds to completely distinct modal shapes.

From experimental modal testing of the pressure vessel, performed at its three loading states, the natural frequencies (Table 8) and damping ratios (Table 9) of individual modes of the vessel's vibration were obtained.

Table 8. Natural frequencies of the vessel obtained for different levels of internal pressure by EMA. $^{\alpha}$, $^{\beta}$ = repeated modes; † = mode was not found.

Estimated Natural Frequency (Hz)										
Pressure	**Mode 1**	**Mode 2**	**Mode 3**	**Mode 4**	**Mode 5**	**Mode 6**	**Mode 7**	**Mode 8**	**Mode 9**	**Mode 10**
80 bar	1788 $^{\alpha}$	2489 $^{\alpha}$	3923 $^{\alpha}$	4146	4533 $^{\alpha}$	4945 $^{\alpha}$	5560 $^{\alpha}$	6113 $^{\alpha}$	6347 $^{\alpha}$	†
	1794 $^{\beta}$	2490 $^{\beta}$	3935 $^{\beta}$	†	4536 $^{\beta}$	4948 $^{\beta}$	5571 $^{\beta}$	6141 $^{\beta}$	6356 $^{\beta}$	†
40 bar	1734 $^{\alpha}$	2365 $^{\alpha}$	3849 $^{\alpha}$	4006	4522 $^{\alpha}$	4823 $^{\alpha}$	5581 $^{\alpha}$	6068 $^{\alpha}$	6204 $^{\alpha}$	6359
	1740 $^{\beta}$	2367 $^{\beta}$	3860 $^{\beta}$	†	4524 $^{\beta}$	4830 $^{\beta}$	5596 $^{\beta}$	6095 $^{\beta}$	6215 $^{\beta}$	†
0 bar	1665 $^{\alpha}$	2209 $^{\alpha}$	3754 $^{\alpha}$	3830	4501 $^{\alpha}$	4677 $^{\alpha}$	5593 $^{\alpha}$	6009 $^{\alpha}$	6033 $^{\alpha}$	6222 $^{\alpha}$
	1673 $^{\beta}$	2211 $^{\beta}$	3765 $^{\beta}$	†	4504 $^{\beta}$	4685 $^{\beta}$	5617 $^{\beta}$	6028 $^{\beta}$	6044 $^{\beta}$	6248 $^{\beta}$

Table 9. Damping ratios of the vessel's modes obtained for different levels of internal pressure by EMA. $^{\alpha}$, $^{\beta}$ = repeated modes; † = mode was not found.

Estimated Damping Ratio (%)										
Pressure	**Mode 1**	**Mode 2**	**Mode 3**	**Mode 4**	**Mode 5**	**Mode 6**	**Mode 7**	**Mode 8**	**Mode 9**	**Mode 10**
80 bar	0.1101 $^{\alpha}$	0.0941 $^{\alpha}$	0.0877 $^{\alpha}$	0.0847	0.0773 $^{\alpha}$	0.0759 $^{\alpha}$	0.0622 $^{\alpha}$	0.0872 $^{\alpha}$	0.0771 $^{\alpha}$	†
	0.1201 $^{\beta}$	0.0948 $^{\beta}$	0.0881 $^{\beta}$	†	0.0785 $^{\beta}$	0.0757 $^{\beta}$	0.0609 $^{\beta}$	0.0877 $^{\beta}$	0.0792 $^{\beta}$	†
40 bar	0.1015 $^{\alpha}$	0.0818 $^{\alpha}$	0.0621 $^{\alpha}$	0.0613	0.0574 $^{\alpha}$	0.0660 $^{\alpha}$	0.0503 $^{\alpha}$	0.0743 $^{\alpha}$	0.0662 $^{\alpha}$	0.0610
	0.1007 $^{\beta}$	0.0831 $^{\beta}$	0.0649 $^{\beta}$	†	0.0581 $^{\beta}$	0.0631 $^{\beta}$	0.0483 $^{\beta}$	0.0760 $^{\beta}$	0.0648 $^{\beta}$	†
0 bar	0.0579 $^{\alpha}$	0.0499 $^{\alpha}$	0.0453 $^{\alpha}$	0.0420	0.0458 $^{\alpha}$	0.0442 $^{\alpha}$	0.0410 $^{\alpha}$	0.0465 $^{\alpha}$	0.0466 $^{\alpha}$	0.0439 $^{\alpha}$
	0.0593 $^{\beta}$	0.0503 $^{\beta}$	0.0469 $^{\beta}$	†	0.0436 $^{\beta}$	0.0448 $^{\beta}$	0.0403 $^{\beta}$	0.0474 $^{\beta}$	0.0469 $^{\beta}$	0.0469 $^{\beta}$

The vessel's modal shapes obtained for all three loading states did not differ significantly. Figure 12 shows ten deformation modal shapes (excluding modal shapes of the repeated modes denoted in Table 8 by β) that were observed in the selected frequency span of 0–6400 Hz. Mode 10 was not identified for the loaded vessel (80 bar) because its natural frequency exceeds the analyzed frequency span. When comparing the results of 80 bar and 0 bar loading states, a decrease of up to 11.3% can be seen for almost all natural frequencies. This change did not occur only for Mode 7, even though its natural frequency increased by 0.6–0.8%. However, this mode differed in character from the others due to significant vibration in the valve region visible from the numerical analysis results (Section 3.2).

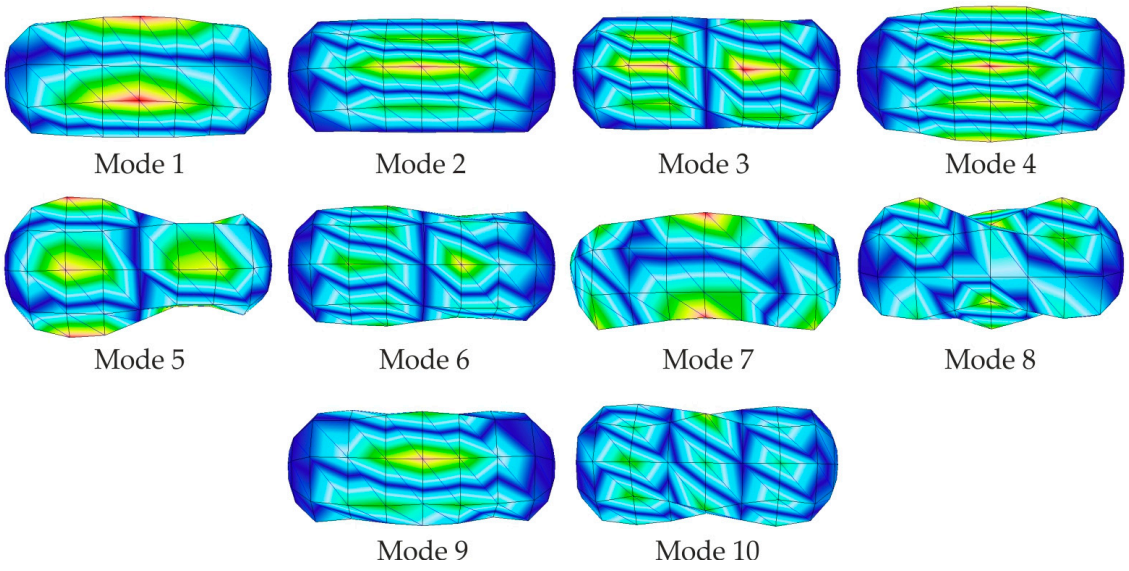
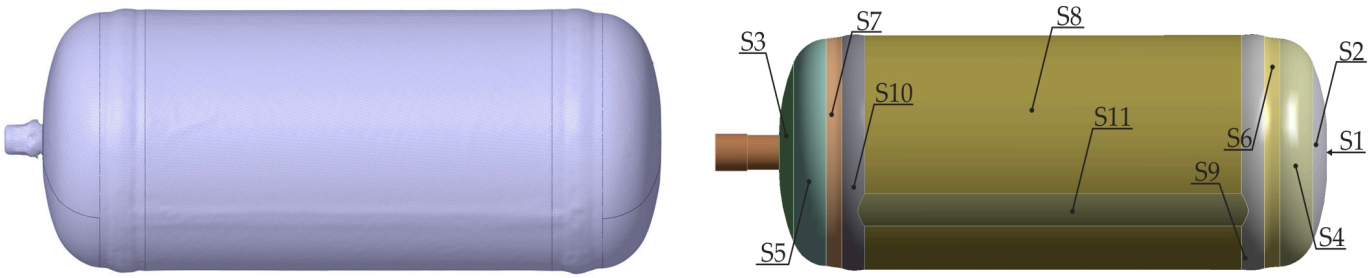


Figure 12. Modal modes of the analyzed pressure vessel estimated by EMA in the selected frequency span of 0–6400 Hz. For all the estimated repeated modes, the figure shows only one mode determined at the first singular curve of the CMIF plot.

3.2. Numerical Modal Analysis of the Pressure Vessel

After performing the last modal testing (vessel with 0 bar pressure), the authors formulated a numerical analysis based on FEM. To create the most accurate numerical model possible, the outer surface of the pressure vessel (Figure 13a) was scanned using a handheld 3D scanner EXAscan (Creaform Inc., Lévis, QC, Canada). Using the obtained outer contour, a shell model of the vessel was created. The choice of the shell model was based on the consideration of simplifying computationally intensive optimization processes and the possible reduction in time requirements. Since pressure vessels generally may not have the same thickness in every cross-section, the authors decided to divide the created numerical model into surfaces labeled S1 to S11, whose thicknesses could be different. In addition, the numerical model included a part on the left simulating a thread-reducing nut, to which a manometer determining the internal pressure of the medium was connected to the vessel valve. The thread-reducing nut was not disconnected from the vessel during the modal testing, and it caused an increase in the weight of the analyzed vessel to 1768 g. After the mesh convergence analysis, a shell mesh consisting of eight-node quadratic elements (SHELL281) of 2 mm average size was created on the model. The total number of elements and nodes defined was 22,688 and 65,209, respectively.



(**a**) (**b**)

Figure 13. Analyzed pressure vessel: (**a**) scanned outer surface; (**b**) numerical shell model with labeled S1 to S11 surfaces representing parts of the vessel with potentially different wall thicknesses.

Since no information about the material of the vessel was available at that time, it was necessary to obtain it. To perform chemical and mechanical tests on samples of the vessel material, the vessel was cut into several parts (Figure S1, Supplementary Materials). In the first step of material identification, an MIRA 3 FE-SEM scanning electron microscope (TESCAN GROUP, a.s., Brno-Kohoutovice, Czech Republic) with an EDX detector (Oxford Instruments, Abingdon, UK) was used. By analyzing the spectrum (Figure S2a, Supplementary Materials), a basic element analysis was performed, the result of which (Figure S2b, Supplementary Materials) predicted that the material of the pressure vessel was steel.

In the next phase of material testing, a more detailed element analysis was performed in combination with mechanical testing to obtain information about the grade of steel. Based on the results obtained by both methods (Table 10), the steel grade of the vessel material was estimated at P355NB, which was also confirmed by the pressure vessel manufacturer.

After identifying the material properties, a numerical modal analysis was performed on a freely constrained shell model of the unloaded vessel (0 bar inner pressure) with initially defined thicknesses of surfaces S1 to S11, and the mass of the obtained numerical model approximately corresponded to its actual value of 1768 g (mass of the vessel + thread-reducing nut). The thicknesses Ti, defined by the authors (for i = 1 up to 11, corresponding to the surfaces S1 to S11), were as follows:

- T_1 = 1.9 mm;
- T_2 = T_3 = 2.0 mm;

- $T_4 = T_5 = 2.1$ mm;
- $T_6 = T_7 = 2.2$ mm;
- $T_8 = 2.5$ mm;
- $T_9 = T_{10} = T_{11} = 2.9$ mm.

Table 10. Chemical composition of the analyzed vessel material and its mechanical properties.

	Material Testing							
Chemical composition of the material (%)	Fe 97.898	Mn 1.4566	Si 0.1986	C 0.1974	Ti 0.0148	Nb 0.0052	P 0.0044	S <0.001
Mechanical properties of the material	Yield Strength = 365 MPa Tensile Strength = 540 MPa Modulus of Elasticity = 200,000 MPa Density = 7850 kg/m^3							

The mass of the initially created numerical shell model was 1697.6 g. Subsequently, parametric optimization was performed with 11 design variables, i.e., the thicknesses of surfaces T_1 to T_{11}. The MOGA method was chosen as the optimization method. Since the number of design variables was significantly higher than in previous cases, a larger number of estimated design points was also selected in the ANSYS software, i.e., the total number of design points was 546, with 95 samples generated initially and 95 samples per iteration, finding three candidates in a maximum of seven iterations. The optimization objectives were defined as follows:

- To seek a target of 1665 Hz for the natural frequency of the first deformation mode;
- To seek a target of 2209 Hz for the natural frequency of the second deformation mode;
- To seek a target of 3754 Hz for the natural frequency of the third deformation mode;
- To seek a target of 3830 Hz for the natural frequency of the fourth deformation mode;
- To seek a target of 4501 Hz for the natural frequency of the fifth deformation mode;
- To seek a target of 4677 Hz for the natural frequency of the sixth deformation mode;
- To seek a target of 5593 Hz for the natural frequency of the seventh deformation mode;
- To seek a target of 6009 Hz for the natural frequency of the eighth deformation mode;
- To seek a target of 6033 Hz for the natural frequency of the ninth deformation mode;
- To seek a target of 6222 Hz for the natural frequency of the tenth deformation mode.

The ranges of feasible values for individual design parameters were defined in the following way:

- T_1 up to T_7 determined in the range {1.6; 2.5} (mm);
- T_8 determined in the range {1.8; 3.0} (mm);
- T_9 up to T_{11} determined in the range {2.2; 3.2} (mm).

In addition, parameter relationships were defined, specifying that the thickness of surfaces corresponding to welds has to be greater than the thickness of each of their neighboring surfaces. Table 11 shows the updated thicknesses of surfaces T_1 to T_{11} proposed by the ANSYS software. The same table also lists the values of the natural frequencies of the initial and updated shell model of the vessel.

Although after FEMU, Δ_{mean} decreased from 10.48% to 7.46%, the difference in the masses of both numerical models did not reach a significant level. While the actual mass of the vessel was 1768 g, the mass of the updated numerical model was 1705.1 g. According to the authors, the main reason for the lower mass was the bonding (i.e., the type of weld) of the central cylindrical part with the bottom or cover of the vessel, which had not been considered in the previous numerical analyses. According to the EN 12205:2001 standard [30], the weld around the circumference of the vessel can be made according to the methods shown in Figure 14.

Table 11. Comparison of natural frequencies of the vessel (0 bar) obtained using EMA and FEA—initial shell model and shell model after FEMU. $^{\alpha}$, $^{\beta}$ = repeated modes; † = mode was not found; # = difference was not calculated.

Surface	T_i (mm)	EMA	FEA (Initial)		FEA (After FEMU)	
		Freq. (Hz)	Freq. (Hz)	Diff. (%)	Freq. (Hz)	Diff. (%)
S1	1.949	1665 $^{\alpha}$	1603.4 $^{\alpha}$	3.70	1622.9 $^{\alpha}$	2.53
S2	2.048	1673 $^{\beta}$	1610.4 $^{\beta}$	3.74	1630.2 $^{\beta}$	2.56
S3	2.120	2209 $^{\alpha}$	2126.3 $^{\alpha}$	3.74	2229.7 $^{\alpha}$	0.94
S4	2.170	2211 $^{\beta}$	2147.5 $^{\beta}$	2.87	2246.4 $^{\beta}$	1.60
S5	2.164	3754 $^{\alpha}$	3088.0 $^{\alpha}$	17.74	3457.4 $^{\alpha}$	7.90
S6	2.110	3765 $^{\beta}$	3089.0 $^{\beta}$	17.95	3458.6 $^{\beta}$	8.14
S7	2.193	3830	3558.5 $^{\alpha}$	7.09	3635.1 $^{\alpha}$	5.09
S8	2.488	†	3578.7 $^{\beta}$	#	3659.8 $^{\beta}$	#
S9	2.895	4501 $^{\alpha}$	3734.8 $^{\alpha}$	17.02	3941.8 $^{\alpha}$	12.42
S10	2.972	4504 $^{\beta}$	3770.8 $^{\beta}$	16.28	3967.2 $^{\beta}$	11.92
S11	2.901	4677 $^{\alpha}$	4425.2 $^{\alpha}$	5.38	4463.4 $^{\alpha}$	4.57
		4685 $^{\beta}$	4439.2 $^{\beta}$	5.25	4473.7 $^{\beta}$	4.51
		5593 $^{\alpha}$	4441.9 $^{\alpha}$	20.58	4626.1 $^{\alpha}$	17.29
		5617 $^{\beta}$	4460.8 $^{\beta}$	20.58	4652.6 $^{\beta}$	17.17
		6009 $^{\alpha}$	4523.7 $^{\alpha}$	24.72	4866.6 $^{\alpha}$	19.01
		6028 $^{\beta}$	5566.6 $^{\beta}$	7.65	5576.8 $^{\beta}$	7.49
		6033 $^{\alpha}$	5582.2 $^{\alpha}$	7.47	5590.1 $^{\alpha}$	7.34
		6044 $^{\beta}$	5790.8 $^{\beta}$	4.19	5873.2 $^{\beta}$	2.83
		6222 $^{\alpha}$	5808.6 $^{\alpha}$	6.64	5910.3 $^{\alpha}$	5.01
		6248 $^{\beta}$	5838.7 $^{\beta}$	6.55	6028.6 $^{\beta}$	3.51
		Δ_{mean}:		10.48		7.46

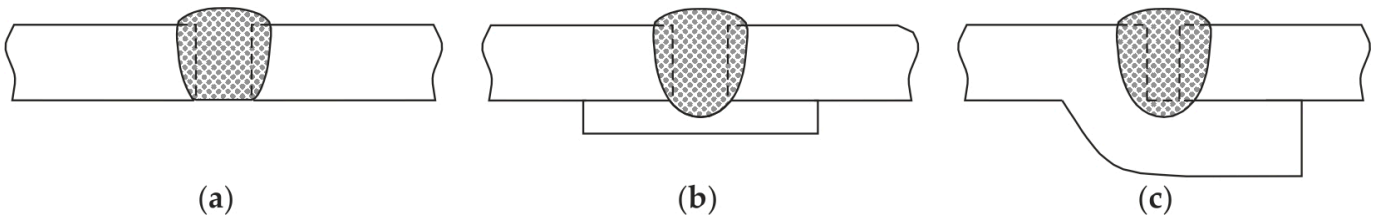


Figure 14. Types of welds in pressure vessel parts according to EN 12205:2001: (**a**) butt weld; (**b**) butt weld with an underlay; (**c**) overlap weld joint.

Based on the cutting-up of the vessel, it was found that the parts of the analyzed vessel were bonded by an overlap weld joint (Figure S1, Supplementary Materials). Since such a bond not only contributes to the total mass but can also affect the modal parameters of the vessel due to its reinforcing effect, the authors decided to create a 3D model of the vessel (Figure 15) based on the geometric parameters obtained in the previous step. After mesh convergence analysis, the mesh consisted of 347,817 ten-node 3D solid elements (SOLID187) of 2 mm size with quadratic approximation and 174,948 nodes. The mesh was refined in the locations of overlap weld joints, where the element size was equal to 1 mm.

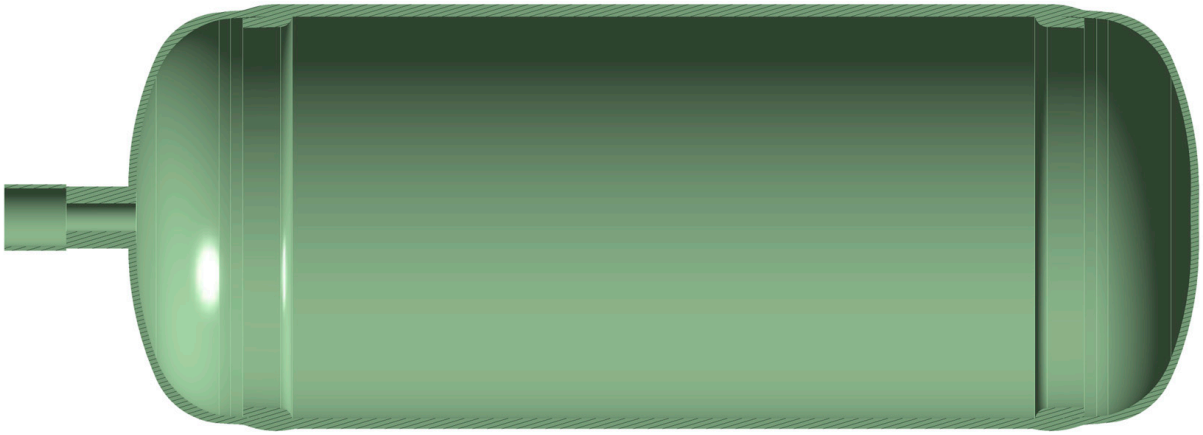


Figure 15. Cross-section of the 3D numerical model of the vessel.

A pre-stress modal analysis was then performed on the created 3D model. Based on model updating, performed according to the parameters as specified for the shell model, the thicknesses of surfaces T_1 to T_{11} designed for the 3D model of the vessel (Table 12 on the left) without loading (0 bar state) were obtained. After subsequent numerical pre-stress modal analyses of the vessel, realized with updated thicknesses T_1 to T_{11} for all analyzed loading states, the natural frequencies obtained were compared with the natural frequencies of the vessel obtained by EMA (Table 12 on the right).

Table 12. Comparison of natural frequencies of the vessel for different internal pressure levels obtained using EMA and FEA—3D model after FEMU. $^{\alpha}$, $^{\beta}$ = repeated modes; † = mode was not found; # = difference was not calculated.

Surf.	T_i (After FEMU) (mm)	EMA (80 Bar)	FEA (80 Bar)		EMA (40 Bar)	FEA (40 Bar)		EMA (0 Bar)	FEA (0 Bar)	
		Freq. (Hz)	Freq. (Hz)	Diff. (%)	Freq. (Hz)	Freq. (Hz)	Diff. (%)	Freq. (Hz)	Freq. (Hz)	Diff. (%)
S1	1.791	1788 $^{\alpha}$	1800.2 $^{\alpha}$	0.68	1734 $^{\alpha}$	1728.1 $^{\alpha}$	0.34	1665 $^{\alpha}$	1654.9 $^{\alpha}$	0.61
S2	1.898	1794 $^{\beta}$	1804.6 $^{\beta}$	0.59	1740 $^{\beta}$	1733.3 $^{\beta}$	0.39	1673 $^{\beta}$	1660.7 $^{\beta}$	0.74
S3	1.911	2489 $^{\alpha}$	2537.2 $^{\alpha}$	1.94	2365 $^{\alpha}$	2381.9 $^{\alpha}$	0.71	2209 $^{\alpha}$	2219.9 $^{\alpha}$	0.49
S4	2.718	2490 $^{\beta}$	2547.4 $^{\beta}$	2.31	2367 $^{\beta}$	2394.0 $^{\beta}$	1.14	2211 $^{\beta}$	2234.3 $^{\beta}$	1.05
S5	2.744	3923 $^{\alpha}$	3986.3 $^{\alpha}$	1.61	3849 $^{\alpha}$	3886.1 $^{\alpha}$	0.96	3754 $^{\alpha}$	3785.7 $^{\alpha}$	0.84
S6	1.812	3935 $^{\beta}$	3997.5 $^{\beta}$	1.59	3860 $^{\beta}$	3898.3 $^{\beta}$	0.99	3765 $^{\beta}$	3799.0 $^{\beta}$	0.90
S7	1.784	4146	4192.4 $^{\alpha}$	1.12	4006	4009.8 $^{\alpha}$	0.09	3830	3823.4 $^{\alpha}$	0.17
S8	2.512	†	4213.7 $^{\beta}$	#	†	4033.6 $^{\beta}$	#	†	3849.8 $^{\beta}$	#
S9	2.898	4533 $^{\alpha}$	4511.4 $^{\alpha}$	0.48	4522 $^{\alpha}$	4480.5 $^{\alpha}$	0.92	4501 $^{\alpha}$	4450.1 $^{\alpha}$	1.13
S10	2.906	4536 $^{\beta}$	4511.7 $^{\beta}$	0.54	4524 $^{\beta}$	4480.9 $^{\beta}$	0.95	4504 $^{\beta}$	4450.7 $^{\beta}$	1.18
S11	2.957	4945 $^{\alpha}$	5044.9 $^{\alpha}$	2.02	4823 $^{\alpha}$	4890.2 $^{\alpha}$	1.39	4677 $^{\alpha}$	4734.4 $^{\alpha}$	1.23
		4948 $^{\beta}$	5064.4 $^{\beta}$	2.35	4830 $^{\beta}$	4911.5 $^{\beta}$	1.69	4685 $^{\beta}$	4757.7 $^{\beta}$	1.55
		5560 $^{\alpha}$	5511.5 $^{\alpha}$	0.87	5581 $^{\alpha}$	5506.3 $^{\alpha}$	1.34	5593 $^{\alpha}$	5501.4 $^{\alpha}$	1.64
		5571 $^{\beta}$	5522.7 $^{\beta}$	0.87	5596 $^{\beta}$	5517.6 $^{\beta}$	1.40	5617 $^{\beta}$	5512.8 $^{\beta}$	1.86
		6113 $^{\alpha}$	6075.5 $^{\alpha}$	0.61	6068 $^{\alpha}$	6006.3 $^{\alpha}$	1.02	6009 $^{\alpha}$	5937.9 $^{\alpha}$	1.18
		6141 $^{\beta}$	6085.4 $^{\beta}$	0.91	6095 $^{\beta}$	6016.6 $^{\beta}$	1.29	6028 $^{\beta}$	5948.6 $^{\beta}$	1.32
		6347 $^{\alpha}$	6384.9 $^{\alpha}$	0.60	6204 $^{\alpha}$	6191.1 $^{\alpha}$	0.21	6033 $^{\alpha}$	5996.0 $^{\alpha}$	0.61
		6356 $^{\beta}$	6420.3 $^{\beta}$	1.01	6215 $^{\beta}$	6229.1 $^{\beta}$	0.23	6044 $^{\beta}$	6036.8 $^{\beta}$	0.12
		†	6562.9 $^{\alpha}$	#	6359	6440.8 $^{\alpha}$	1.29	6222 $^{\alpha}$	6319.4 $^{\alpha}$	1.57
		†	6584.8 $^{\beta}$	#	†	6464.1 $^{\beta}$	#	6248 $^{\beta}$	6344.1 $^{\beta}$	1.54
		Δ_{mean}:		1.18			0.91			1.04

Based on the results obtained, it can be stated that after performing optimization processes and modifying the numerical 3D model of the vessel, a very good match in

the compared parameters was achieved. The mass of the created numerical 3D model determined by the ANSYS software was 1780.2 g, which exceeds the actual value by only 12.2 g (0.7%). Mean differences of up to 1.2% between the natural frequency values of the vessel obtained by experimental and numerical modal analysis were achieved. A very good qualitative match can also be observed in the modal shapes obtained numerically (Figure 16) and experimentally (Figure 12), respectively.

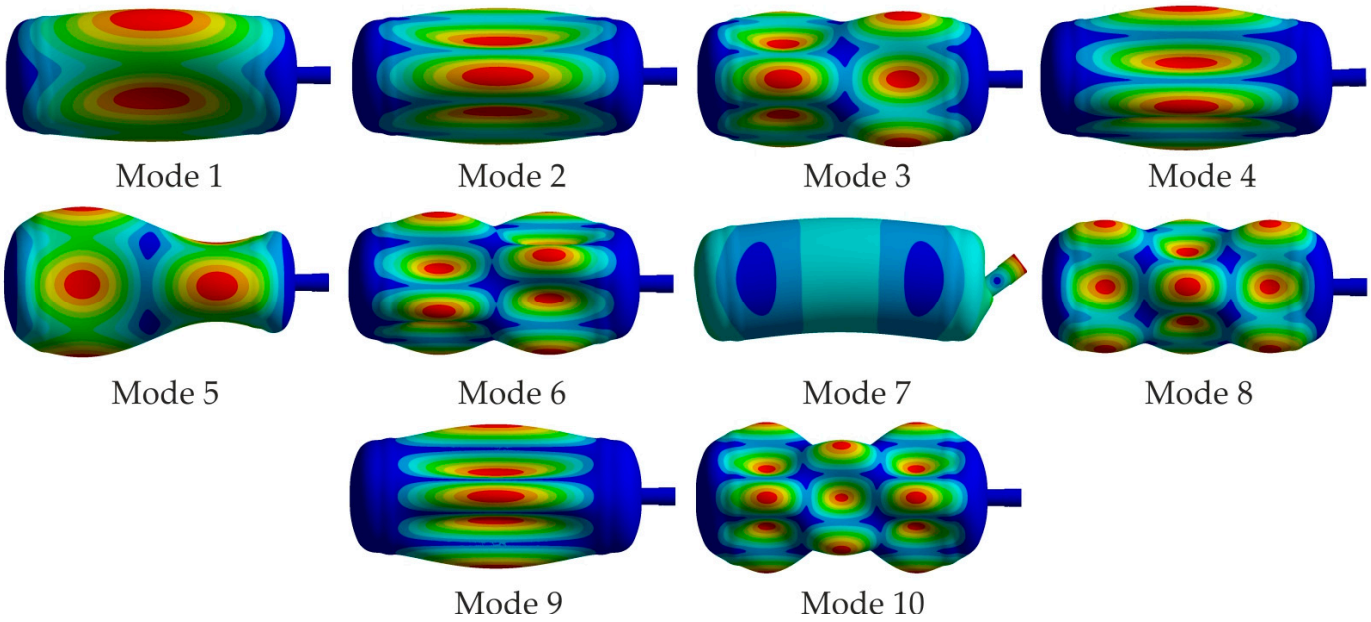


Figure 16. Deformation modal shapes of the updated 3D vessel's numerical model with modeled overlap weld joints obtained by FEA in the selected frequency span of 0–6400 Hz. For all the pairs of calculated repeated modes, the figure shows only the first, i.e., α mode.

4. Discussion

The article describes the methodology for updating finite element models of axisymmetric structures based on data obtained from modal testing. Two approaches can be characterized in this methodology, namely experimental and numerical ones. The experimental approach is important in terms of obtaining reference data, i.e., frequency response functions (FRFs), estimated modal parameters (natural frequencies, damping ratios, or modal shapes), and geometric or material characteristics of the analyzed structure. For that reason, it is necessary to choose measurement methods and to define measurement conditions in such a way that the obtained data are affected minimally by negative factors influencing their final accuracy.

The article describes an experimental modal analysis performed on two freely constrained structures. This type of constraint, provided by the authors by suspending the analyzed structures using flexible rubber strings, was chosen to eliminate the impact of fixture modes, friction, and most damping, respectively. To obtain the FRFs, multiple input multiple output (MIMO) measurements were performed using a fixed embedded accelerometer and roving hammer-impact method. An adequate number of degrees of freedom (DOFs) and reference DOFs, with the application of the linear peak hold average method of the fast Fourier transform (FFT) signals, led to an increase in the accuracy of the FRFs. To estimate modes with closely spaced frequencies or repeated modes, the authors chose the Complex Mode Indicator Function based on the Singular Value Decomposition (SVD) method and the auto MAC for their validation. Based on the above, the individual vibration modes (containing information about natural frequencies, damping ratios and modal shapes) of the analyzed structures were easily identified and separated. In both

cases, information was obtained on ten vibration modes, including repeated ones, which were identified in 80% and 90% of the modes, respectively. The data obtained in this way was a suitable article with sufficient accuracy for performing finite element model updating (FEMU).

Finite element model updating was performed in the ANSYS Mechanical 2024 R1 software using step-by-step iterative optimization, whereby the possibilities of solving the problem with one or more design variables in the form of geometric quantities were pointed out. Using a numerical 3D model of a steel pipe, the authors analyzed the influence of various ranges of design variables' feasible values on the resulting mean difference Δ_{mean} obtained in natural frequencies, weight m_{num}, and wall thickness t of the numerical model. Based on Table 13, which presents the observed parameters, it can be concluded that by gradually adjusting the ranges, it was possible to update the dimensions of the numerical model so that the mean difference in natural frequencies reached a level of up to 1.5%, with a maximum level of about 4%. In both cases, the obtained models approached the actual values in terms of weight (m_{actual} = 3916 g) and nominal wall thickness (T = 1.5 mm).

Table 13. Comparison of observed parameters of the steel pipe FEMU model obtained for various defined numbers of design variables and ranges of their feasible values.

Design Variables' Range of Feasible Values		Observed Parameters				
r_o (mm)	r_i (mm)	$Diff_{max}$ (%)	$Diff_{min}$ (%)	Δ_{mean} (%)	m_{num} (g)	t (mm)
{60.001; 67}	{60}	10.95	2.4	8.04	3536	1.313
{60.001; 63}	{60}	10.95	2.4	8.04	3536	1.313
{60.001; 62}	{60}	3.76	1.17	2.84	3866	1.434
{60.001; 61.8}	{60}	3.83	0.06	1.26	3983	1.477
{60.001; 61.6}	{60}	3.42	0.32	1.32	4014	1.489
{60.001; 65}	{55; 60}	91.65	17.69	57.17	7812	2.873
{60.001; 62.5}	{57.5; 60}	32.27	13.54	19.39	5204	1.936
{60.6; 62}	{59.5; 60.5}	4.01	0.15	1.49	3900	1.458

In the next section, the authors focused on validating the described methodology, specifically for the FEMU of a pressure vessel used to store a gas medium. In addition to updating the numerical model, the authors also aimed to highlight the possibility of identifying unknown geometric quantities. In order to make the numerical model as accurate as possible, the authors used scanning, detection, spectral analysis, and material testing methods to determine the material of the vessel and its mechanical properties. The outer surface of the vessel was also scanned using a 3D scanner, and the data obtained was used to create an initial numerical shell model of the vessel, which needed to be updated. It should be noted that the number of design variables, i.e., the thicknesses of the defined surfaces of the vessel, was eleven, which is much higher than in the pipe case. In the case of the shell model, only a partial match with the actual natural frequencies of the vessel was achieved (Table 14). The authors considered the main reason to be the absence of consideration of the weld-creating method between the cylindrical part of the vessel and its bottom and cover. After creating a 3D model considering overlapping weld joints, the match between the natural frequencies obtained experimentally and numerically was significantly higher (mean difference of 1.04%). It is assumed that the improvement in results was not caused solely by the change in local stiffness and mass at the welds, but by a combination of several factors, namely the use of 3D solid elements, the addition of local stiffness and mass, and overall mass redistribution. The result of the optimization process, i.e., the updated thicknesses of eleven surfaces obtained for the model without load (0 bar),

was also applied in the case of the numerical models loaded with pressures of 40 bar and 80 bar, respectively. In each case, the results obtained were very accurate. The mass of the updated model differed only minimally from the mass of the actual vessel (Table 14).

Table 14. Comparison of observed parameters of the pressure vessel FEMU model obtained for shell and 3D models.

Model Type	Observed Parameters				
	$Diff_{max}$ (%)	$Diff_{min}$ (%)	Δ_{mean} (%)	m_{num} (g)	m_{actual} (g)
Shell 0 bar (initial)	24.72	2.87	10.48	1697.6	1768
Shell 0 bar (updated)	19.01	0.94	7.46	1705.1	1768
3D model 0 bar (updated)	1.86	0.12	1.04	1780.2	1768
3D model 40 bar (updated)	1.69	0.21	0.91	1780.2	1768
3D model 80 bar (updated)	2.35	0.48	1.18	1780.2	1768

5. Conclusions

This article describes the methodology for FEMU-based identification of dimensions of axisymmetric structures with one, two (reference analysis), or even eleven (validation analysis) design variables. The repeated modes of both analyzed structures, i.e., the pipe and pressure vessel, with split frequencies were obtained from MIMO experimental modal analyses. The main conclusions drawn from the updating process based on the MOGA method can be defined as follows:

- The authors did not neglect or average the repeated modes with split frequencies.
- When selecting the optimization objectives, one of the repeated modes was always selected, specifically the one found on the first singular curve, i.e., the mode with the higher frequency response.
- Using mass as one the optimization functions can lead to improvement in the quality and convergence of the results.
- Significant improvement in the results was obtained after creating and optimization of the vessel 3D model, describing the through-thickness stiffness distribution in the vessel more realistically.
- The modeling of the overlap weld joints causes not only addition of local stiffness and mass but also overall mass redistribution occurring after design variable optimization.

To validate the results obtained, the measurements were carried out at the cut-up vessel using a digital vernier caliper of 0–150 mm range (BGS Technic KG, Wermelskirchen, Germany) and a TG-400 ultrasonic thickness gauge (NDT Systems Inc., Nashua, NH, USA). The measurements were taken at 20 randomly selected points located on individual surfaces of the vessel. The idea was to find the standard deviation of the measured values and thus determine the degree of change in these parameters around the circumference of the vessel. The results obtained can be found in Table 15.

Table 15. Summary of the values of eleven design variables obtained by FEMU and measurements carried out at the cut-up vessel.

Thickness	FEA Shell Initial	FEA Shell Updated	FEA 3D Model Updated	Measurement
T1	1.9 mm	1.949 mm	1.791 mm	1.81 ± 0.02 mm
T2	2.0 mm	2.048 mm	1.898 mm	1.89 ± 0.03 mm
T3	2.0 mm	2.120 mm	1.911 mm	1.88 ± 0.03 mm
T4	2.1 mm	2.170 mm	2.718 mm	2.09 ± 0.07 mm

Table 15. *Cont.*

Thickness	FEA Shell Initial	FEA Shell Updated	FEA 3D Model Updated	Measurement
T5	2.1 mm	2.164 mm	2.744 mm	2.11 ± 0.08 mm
T6	2.2 mm	2.110 mm	1.812 mm	1.92 ± 0.04 mm
T7	2.2 mm	2.193 mm	1.784 mm	1.91 ± 0.03 mm
T8	2.5 mm	2.488 mm	2.512 mm	2.40 ± 0.03 mm
T9	2.9 mm	2.895 mm	2.898 mm	3.08 ± 0.08 mm
T10	2.9 mm	2.972 mm	2.906 mm	3.06 ± 0.11 mm
T11	2.9 mm	2.901 mm	2.957 mm	2.96 ± 0.05 mm

When using 3D model, a good match was achieved for nine of the eleven variables investigated. Only for the T4 and T5 values, which corresponded to the most curved surfaces of the vessel, where also the realized measurements were the most challenging, a lower correlation was achieved. However, it should be noted that these surfaces do not have a constant thickness in the updated 3D numerical model due to connection with neighboring surfaces of different thicknesses. The values 2.718 mm and 2.744 mm, reported as the thicknesses of surfaces S4 and S5 of the updated 3D model, correspond to the thicknesses at their widest cross-sections.

An accurate detection of repeated modes and their splits, together with the proposed methodology, could be applied, e.g., for updating numerical models of damaged axisymmetric structures, for crack detection, or for health monitoring. Although the authors analyzed axisymmetric structures with linear dynamic behavior, it is assumed that under certain conditions, the concept used can also be applied to more complex tasks with local nonlinearities. However, within the scope of these tasks, it is necessary to determine the degree of limitations related not only to the experimental but also to the numerical part of the approach. The analyses would need to focus, e.g., on assessing the smallest measurable frequency split in relation to noise, measurement resolution, and modal identification uncertainty, and quantifying how the size of the crack/character of damage affects the difference in split frequencies. On the other hand, it should be noted that this approach is more suitable for structures of common sizes. To perform modal analysis on large-scale industrial structures, such as hyperbolic cooling towers, silos, or water tanks, it would be necessary to use a different, more suitable type of excitation. Although various natural or ambient sources of dynamic excitation are currently used to perform operational modal analysis, the results obtained do not contain the necessary information about mass-normalized mode shapes. Scaling modes in the case of large-scale objects would only be possible by adding several masses of large magnitude. In addition, optimization methods based on genetic algorithms are robust but computationally extremely intensive. For models of large-scale or complex structures, typically with several million degrees of freedom, the optimization time would grow exponentially.

Supplementary Materials: The following supporting information can be downloaded at: https://www.mdpi.com/article/10.3390/app152111407/s1, Figure S1: Photo of the cut-up pressure vessel; Figure S2: Images related to the material identification of the pressure vessel; Table S1: Design variables feasible range definition and optimization results of the two-variable pipe case without selecting mass as one of the objective functions; Table S2: Natural frequencies of the updated numerical model of the two-variable pipe case without selecting mass as one of the objective functions.

Author Contributions: Conceptualization, M.H. and P.L.; methodology, M.H.; software, P.L., L.H. and J.B.; validation, P.L. and M.H.; formal analysis, J.B.; investigation, M.H. and L.H.; resources, P.L.; writing—original draft preparation, M.H.; visualization, L.H.; supervision, J.B.; funding acquisition, P.L. All authors have read and agreed to the published version of the manuscript.

Funding: This research was funded by the Scientific Grant Agency, Ministry of Education, Science, Research and Sport of the Slovak Republic and the Slovak Academy of Sciences under the projects VEGA 1/0152/24 and VEGA 1/0342/24.

Institutional Review Board Statement: Not applicable.

Informed Consent Statement: Not applicable.

Data Availability Statement: The data that support the findings of this study are available from the corresponding author upon request.

Acknowledgments: The authors would like to thank Viktória Rajťuková from the Department of Biomedical Engineering and Measurement, Technical University of Košice, for the help with preparing the analyzed vessel-scanned model.

Conflicts of Interest: The authors declare no conflicts of interest.

References

1. Brownjohn, J.M.W.; Xia, P.Q. Dynamic assessment of curved cable-stayed bridge by model updating. *J. Struct. Eng.* **2000**, *126*, 252–260. [CrossRef]
2. Brownjohn, J.M.W.; Moyo, P.; Omenzetter, P.; Lu, Y. Assessment of highway bridge upgrading by dynamic testing and finite-element model updating. *J. Bridge Eng.* **2003**, *8*, 162–172. [CrossRef]
3. Friswell, M.I.; Mottershead, J.E. *Finite Element Model Updating in Structural Dynamics*, 1st ed.; Springer: Dordrecht, The Netherlands, 1995.
4. Baruch, M.; Bar-Itzhack, I.Y. Optimal Weighted Orthogonalization of Measured Modes. *AIAA J.* **1978**, *16*, 346–351. [CrossRef]
5. Berman, A. Mass Matrix Correction Using an Incomplete Set of Measured Modes. *AIAA J.* **1979**, *17*, 1147–1148. [CrossRef]
6. Berman, A.; Nagy, E.J. Improvement of a Large Analytical Model Using Test Data. *AIAA J.* **1983**, *21*, 1168–1173. [CrossRef]
7. Mottershead, J.E.; Friswell, M.I. Model Updating in Structural Dynamics: A Survey. *J. Sound Vib.* **1993**, *167*, 347–375. [CrossRef]
8. Lin, R.M.; Ewins, D.J. Analytical model improvement using frequency response functions. *Mech. Syst. Signal Process.* **1994**, *8*, 437–458. [CrossRef]
9. Lin, R.M.; Ewins, D.J. Model Updating Using FRF Data. In Proceedings of the 15th International Seminar on Modal Analysis, Leuven, Belgium, 19–21 September 1990.
10. Esfandiari, A.; Bakhtiari-Nejad, F.; Sanayei, M.; Rahai, A. Structural finite element model updating using transfer function data. *Comput. Struct.* **2010**, *88*, 54–64. [CrossRef]
11. Weng, S.; Xia, Y.; Xu, Y.L.; Zhu, H.P. Substructure based approach to finite element model updating. *Comput. Struct.* **2011**, *89*, 772–782. [CrossRef]
12. Mottershead, J.E.; Link, M.; Friswell, M.I. The sensitivity method in finite element model updating: A tutorial. *Mech. Syst. Signal Process.* **2011**, *25*, 2275–2296. [CrossRef]
13. Lorenzoni, F.; Valluzzi, M.R.; Salvalaggio, M.; Minello, A.; Modena, C. Operational modal analysis for the characterization of ancient water towers in Pompeii. *Procedia Eng.* **2017**, *199*, 3374–3379. [CrossRef]
14. Bru, D.; Ivorra, S.; Baeza, F.J.; Reynau, R.; Foti, D. OMA Dynamic identification of a masonry chimney with severe cracking condition. In Proceedings of the 6th International Operational Modal Analysis Conference, IOMAC15, Gijon, Spain, 12–14 May 2015.
15. Saidin, S.S.; Kudus, S.A.; Jamadin, A.; Anuar, M.A.; Amin, N.M.; Ibrahim, Z.; Zakaria, A.B.; Sugiura, K. Operational modal analysis and finite element model updating of ultra-high-performance concrete bridge based on ambient vibration test. *Case Stud. Constr. Mater.* **2022**, *16*, e01117. [CrossRef]
16. Calayır, Y.; Yetkin, M.; Erkek, H. Finite element model updating of masonry minarets by using operational modal analysis method. *Structures* **2021**, *34*, 3501–3507. [CrossRef]
17. Avci, O.; Alkhamis, K.; Abdeljaber, O.; Alsharo, A.; Hussein, M. Operational modal analysis and finite element model updating of a 230 m tall tower. *Structures* **2022**, *37*, 154–167. [CrossRef]
18. Zhao, J.; Sun, F.; Yang, S.; Yin, W.; Xu, Z.; He, S. Modal characteristics of vertical vibration in typical steel frame structures under road traffic loads: Actual measurements and finite element model update. *J. Build. Eng.* **2025**, *111*, 113346. [CrossRef]
19. Ribeiro, D.; Calçada, R.; Delgado, R.; Brehm, M.; Zabel, V. Finite element model updating of a bowstring-arch railway bridge based on experimental modal parameters. *Eng. Struct.* **2012**, *40*, 413–435. [CrossRef]
20. Yuan, Z.X.; Yu, K.P. Finite element model updating of damped structures using vibration test data under base excitation. *J. Sound Vib.* **2015**, *340*, 303–316. [CrossRef]
21. Adel, F.; Shokrollahi, S.; Jamal-Omidi, M.; Ahmadian, H. A model updating method for hybrid composite/aluminum bolted joints using modal test data. *J. Sound Vib.* **2017**, *396*, 172–185. [CrossRef]

22. Petrone, G.; Meruane, V. Mechanical properties updating of a non-uniform natural fibre composite panel by means of a parallel genetic algorithm. *Compos. Part A Appl. Sci. Manuf.* **2017**, *94*, 226–233. [CrossRef]
23. Cuadrado, M.; Artero-Guerrero, J.A.; Pernas-Sánchez, J.; Varas, D. Model updating of uncertain parameters of carbon/epoxy composite plates from experimental modal data. *J. Sound Vib.* **2019**, *455*, 380–401. [CrossRef]
24. Eiras, J.N.; Payan, C.; Rakotonarivo, S.; Garnier, V. Experimental modal analysis and finite element model updating for structural health monitoring of reinforced concrete radioactive waste packages. *Constr. Build. Mater.* **2018**, *180*, 531–543. [CrossRef]
25. Dimri, A.; Chakraborty, S. Damage identification of reinforced concrete slabs using experimental modal testing and finite element model updating. *Structures* **2024**, *67*, 107023. [CrossRef]
26. Sanz-García, A.; Pernía-Espinoza, A.V.; Fernández-Martínez, R.; Martínez-de-Pisón-Ascacíbar, F.J. Combining genetic algorithms and the finite element method to improve steel industrial processes. *J. Appl. Log.* **2012**, *10*, 298–308. [CrossRef]
27. Zacharia, P.T.; Tsirkas, S.O.; Kabouridis, G.; Yiannopoulos, A.C.; Giannopoulos, G.I. Genetic-Based Optimization of the Manufacturing Process of a Robotic Arm under Fuzziness. *Math. Probl. Eng.* **2018**, *1*, 168014. [CrossRef]
28. Zheng, Q.; Zhu, W.; Zhi, Q.; Sun, H.; Li, D.; Ding, X. Genetic Algorithm Optimization Design of Gradient Conformal Chiral Metamaterials and 3D Printing Verification for Morphing Wings. *Chin. J. Mech. Eng.* **2024**, *37*, 143. [CrossRef]
29. Hagara, M.; Pástor, M.; Lengvarský, P.; Palička, P.; Huňady, R. Modal Parameters Estimation of Circular Plates Manufactured by FDM Technique Using Vibrometry: A Comparative Study. *Appl. Sci.* **2024**, *14*, 10609. [CrossRef]
30. *EN 12205:2001*; Transportable Gas Cylinders—Non-Refillable Metallic Gas Cylinders. European Committee for Standardization: Bruxelles, Belgium, 2015.

Disclaimer/Publisher's Note: The statements, opinions and data contained in all publications are solely those of the individual author(s) and contributor(s) and not of MDPI and/or the editor(s). MDPI and/or the editor(s) disclaim responsibility for any injury to people or property resulting from any ideas, methods, instructions or products referred to in the content.